TUT Magnetic Materials Laboratory Seminar

豊橋技科大磁性研究室セミナー02/07/25

Recent Topics in Magneto-Optics

Linear and nonlinear magneto-optical effects in Fe/Au and Co/Ru superlattices

磁気光学研究の最近の￥話題
Fe/Au, Co/Ru人工格子の線形および非線形磁気光学効果

Katsuaki Sato

Tokyo Univ. Agric. & Technol., Tokyo, Japan

佐藤勝昭 (東京農工大学工学部)

Introduction
はじめに

- Two-types of superlattices
  - TM/Cu, Ag, Au →immiscible; abrupt interface (非固溶;急峻な界面)
  - TM/Pt, Pd→ miscible, gradual interface (固溶系:界面合金化)
- Superlattices and characteristic length (人工格子・多層膜と特性長)
  - L*～λ’(light wavelength光の波長):MO enhancement
  - L*～ds(roughness界面の荒さ)→相互拡散、合金化
  - L*～λ_D(de Broglie wavelenth)→Quantum confinement 量子閉じこめ
  - L*～a (atomic size)→band modificationバンドの改変

Linear magneto-optical effect in Fe/Cu compositionally modulated multilayers Fe/Cu組成変調多層膜の磁気光学効果

- Layer thickness ～ wavelength [波長(λ’)～層厚(d)]
  - Plasma enhancement (プラズマ端でのエンハンス効果)
  - Roughly explained by effective permeability (実効誘電率) $\Psi_K = \frac{\varepsilon_{xy}}{\sqrt{\varepsilon_{xx}}(1-\varepsilon_{xx})}$
  - Multiple reflection and interference(多重反射・干渉効果)
  - Unaccountable for d<a few nm (変調周期が数nm以下になると説明できなくなる)

    mutual diffusion and alloy formation at the interface

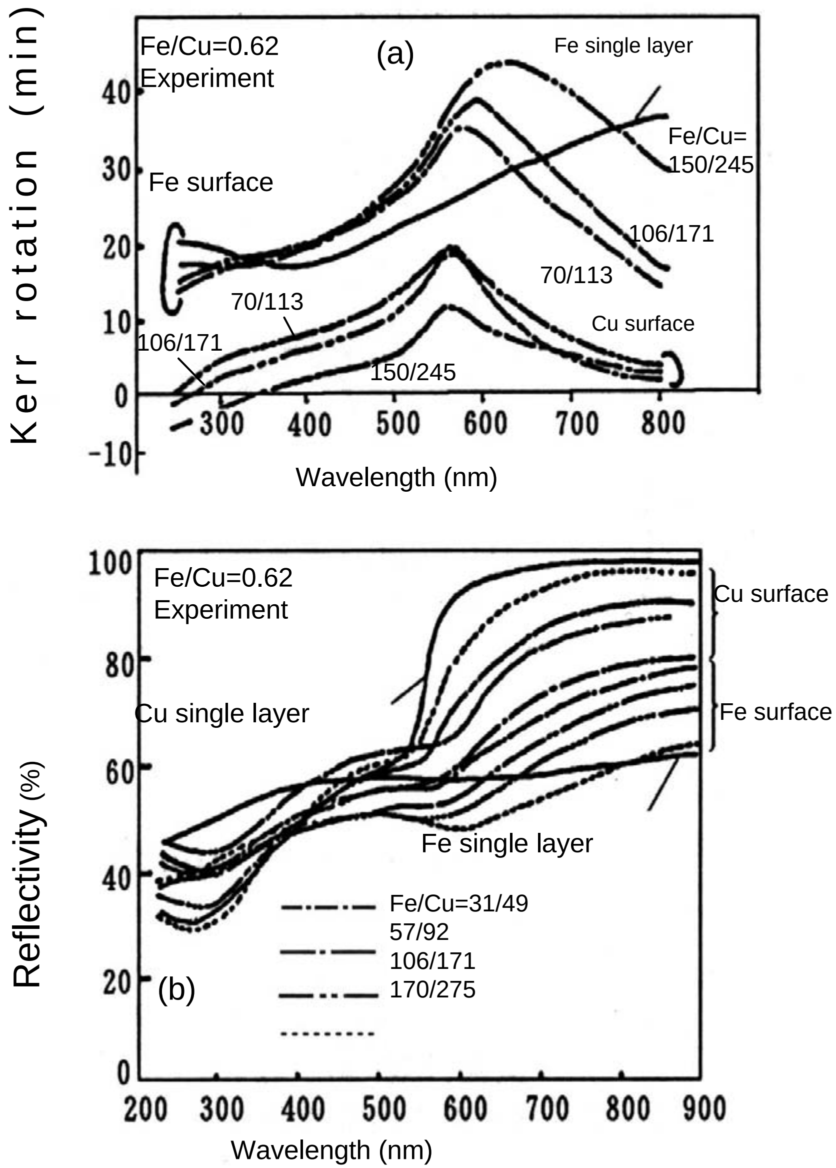

Experimental magneto-optical and reflectivity spectra in Fe/Cu multilayer with different layer thickness

種々の層厚をもったFe/Cu組成変調多層膜の磁気光学スペクトルおよび反射スペクトル（実験値）

Virtual optical constant method(仮想光学定数の方法)

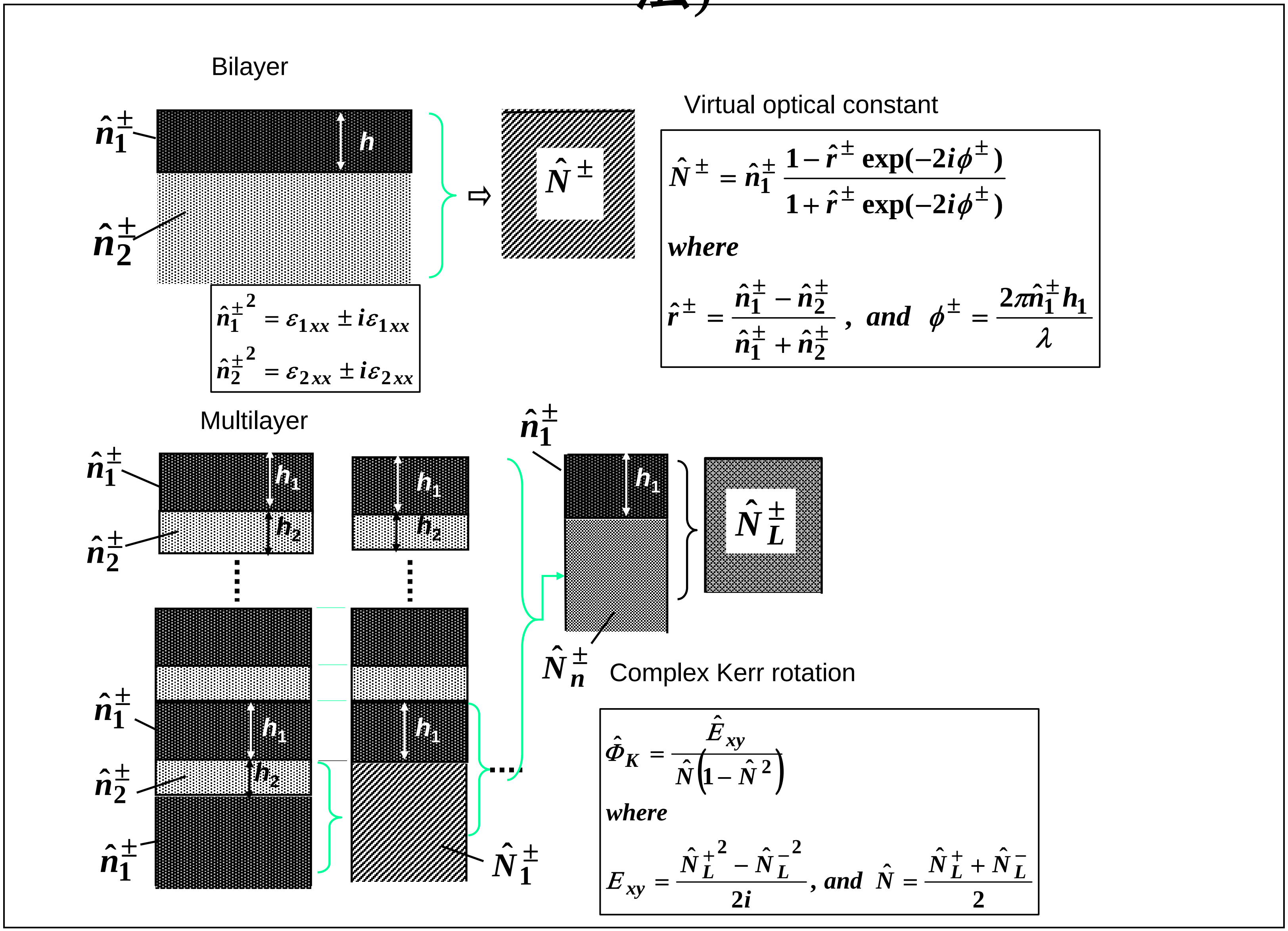

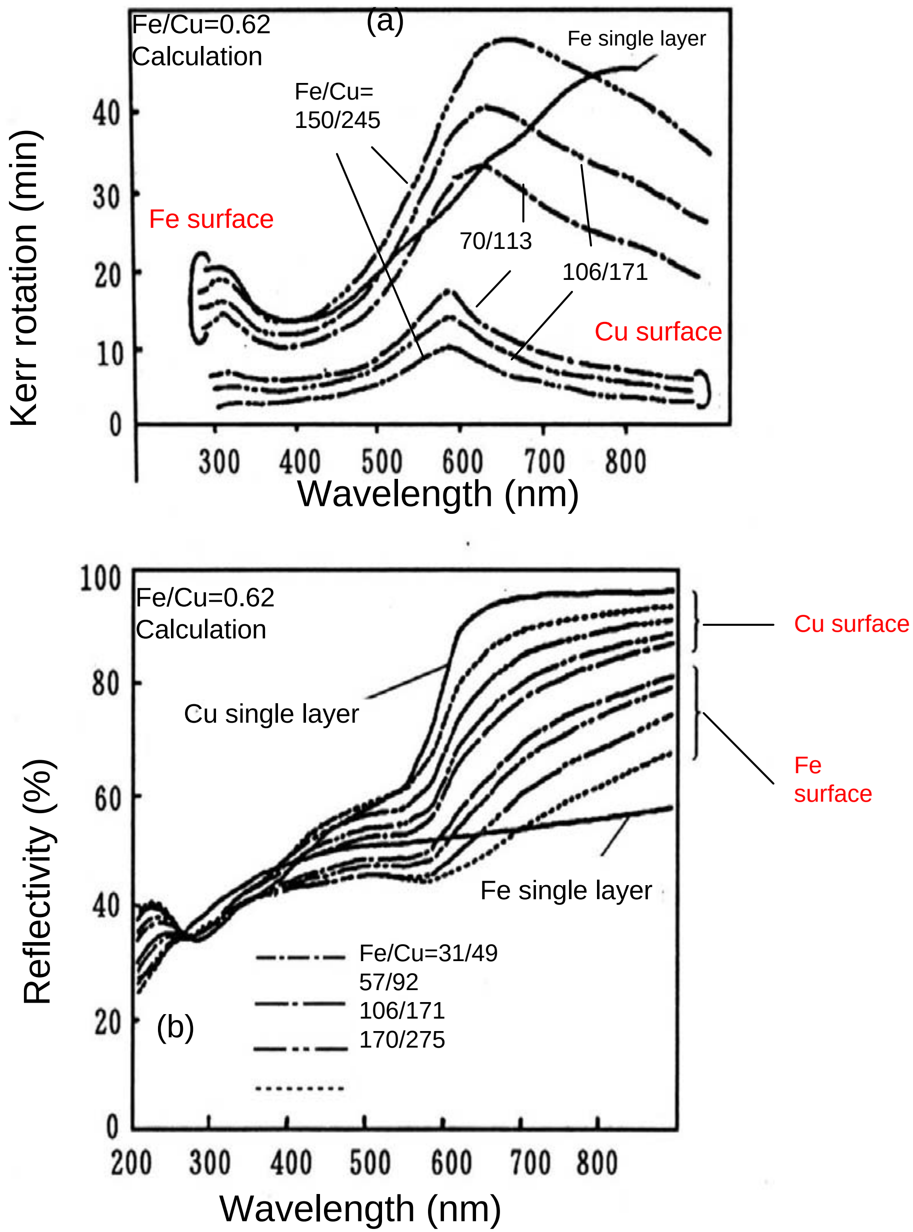

Calculated magneto-optical and reflectivity spectra in Fe/Cu multilayer with different layer thickness

種々の層厚をもったFe/Cu組成変調多層膜の磁気光学スペクトルおよび反射スペクトル（計算値）

Modulation period dependence of Kerr rotation in Fe/Cu multilayers (▲△experiments,solid and broken line: calculation)
Fe/Cu組成変調多層膜のカー回転角の変調周期依存性。

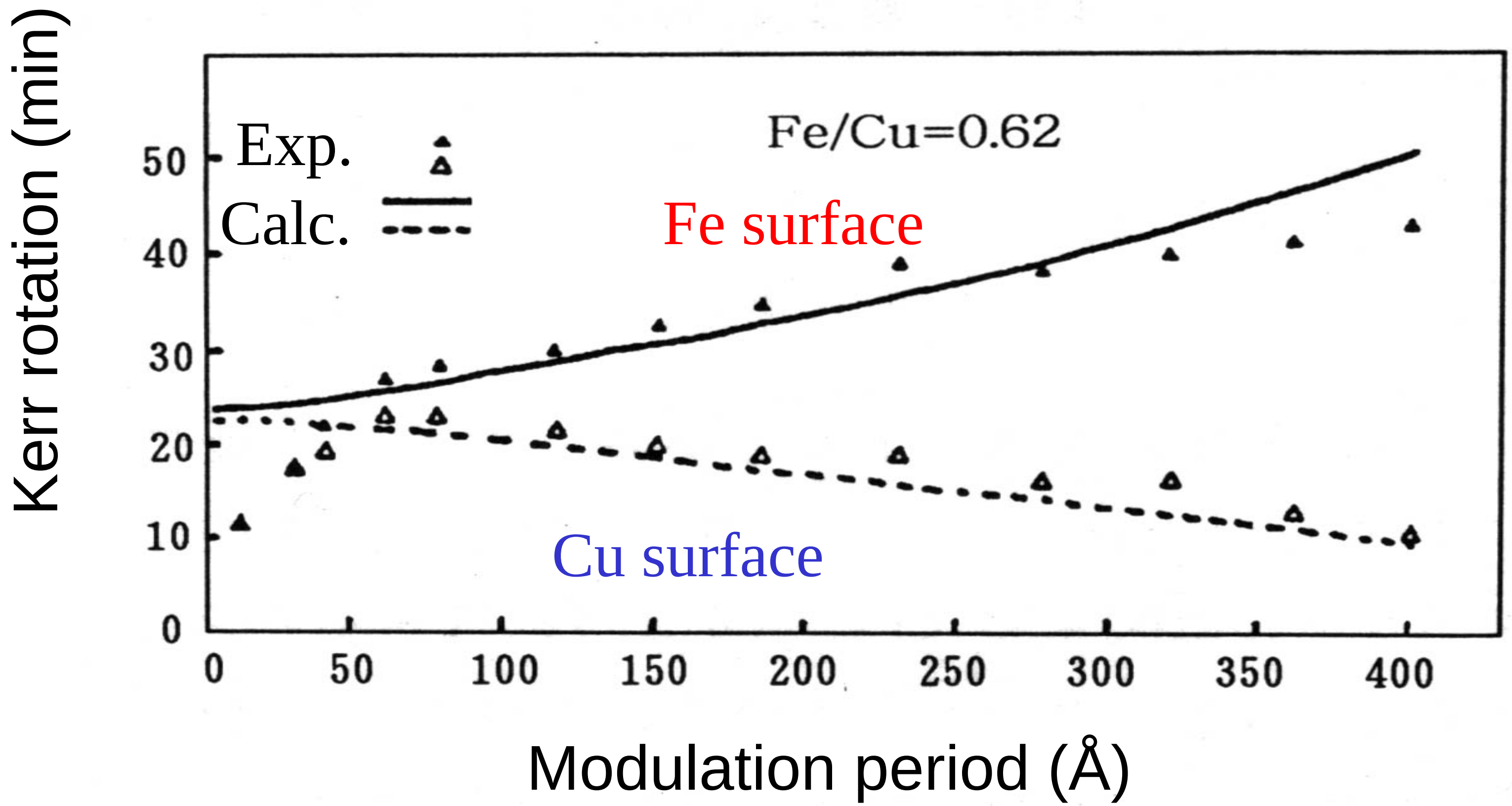

Magneto-optical Effect in Au/Fe/Au trilayer

Au/Fe/Au三層超薄膜の磁気光学効果

- Layer thickness ～ de Broglie wavelength of electrons
  層厚が電子のドブロイ波長と同程度になった場合
- New magneto-optical transition in epitaxially grown Au(cap)/Fe(ultra thin layer)/Au(buffer)/MgO(substrate) trilayer structure
  MBE法でMgO基板上にエピタキシャル成長したAu(100)薄膜の上にFe超薄膜を作製し、その上に保護層としてAuの薄いキャップ層をかぶせた三層膜における新しい光学遷移
- At first the optical structure was assigned to 2D-band.
  Afterward it was re-explained in terms of quantum confinement of electrons in Fe-layer
  当初：2Dのバンドによると同定→その後、Fe層内での電子の量子閉じこめによるとして説明された。

Kerr rotation spectra in Au/Fe/Au ultra thin films

Au/Fe/Au超薄膜の磁気光学カー回転スペクトルのFe層厚依存性

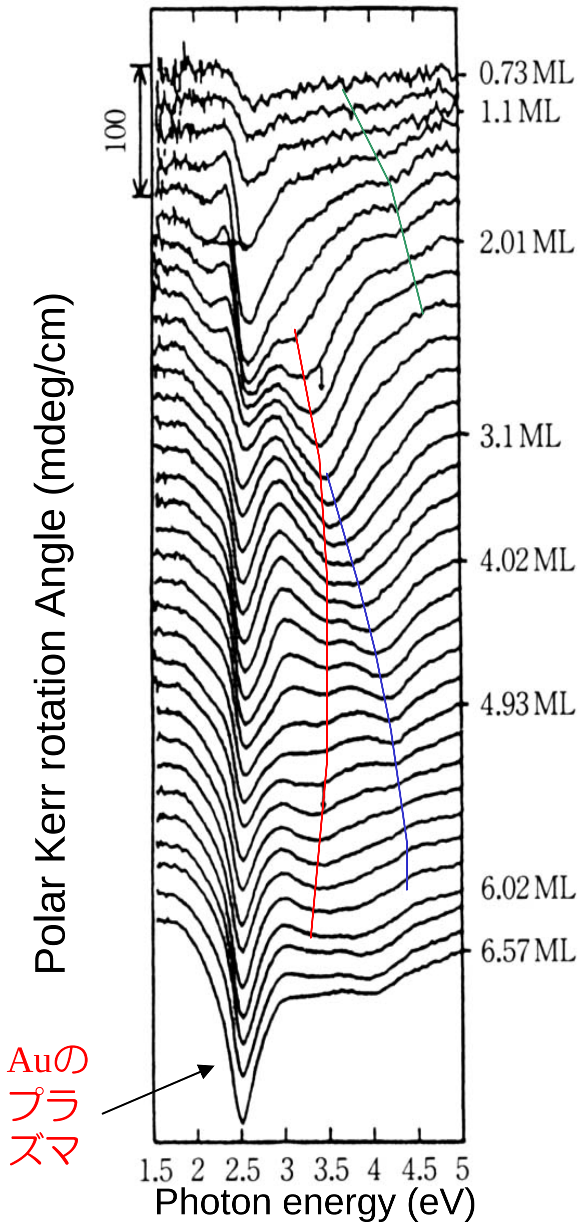

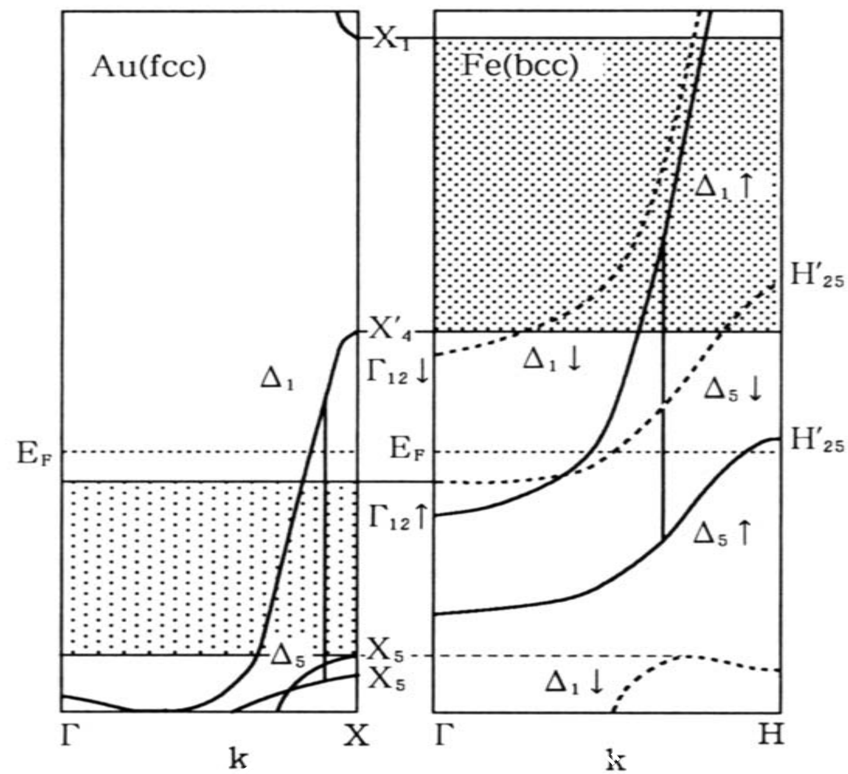

After Y. Suzuki (AIST)

Magneto-optical ellipticity at 4eV vs. thickness of Fe layer

4eVにおける１層あたりのカー楕円率のFe層厚依存性

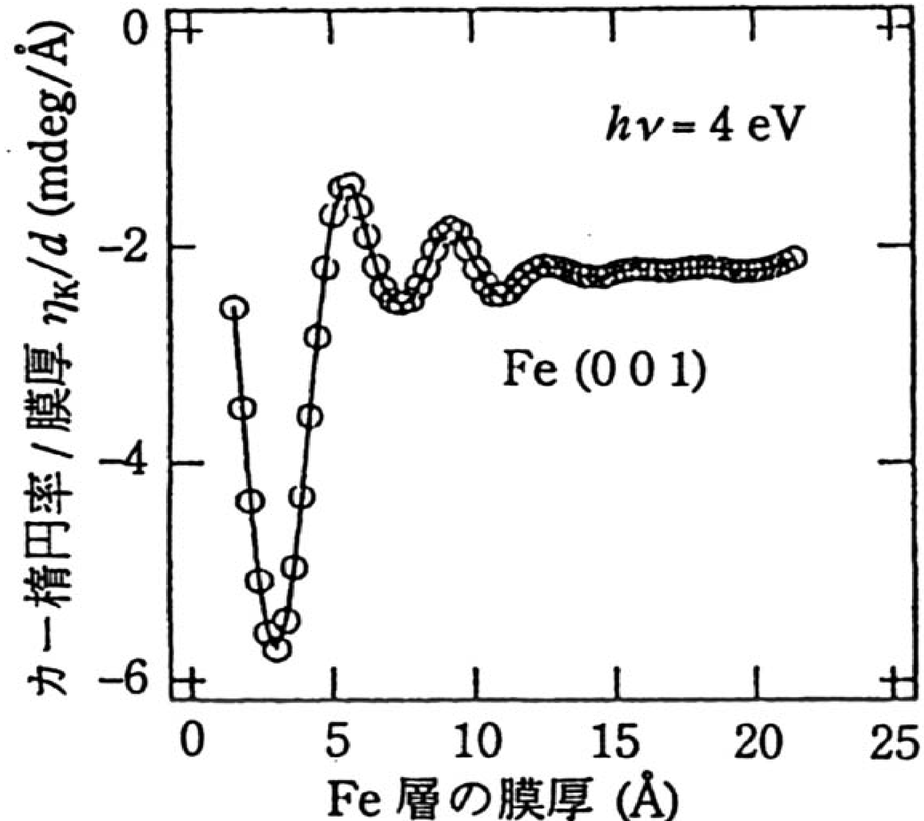

After Y.Suzuki

Au-thickness dependence of Co/Au/Co
Co/Au/Coの磁気光学効果のAu層厚依存性

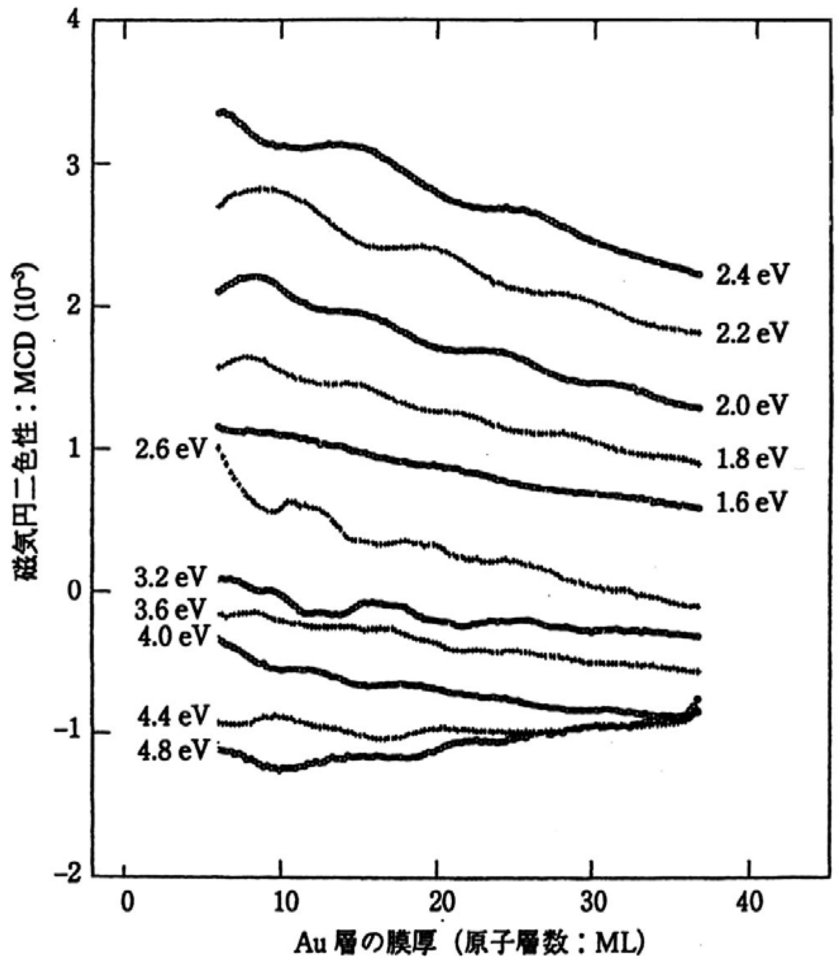

After Y.Suzuki

Artificial ordered alloy of Fe/Au
Fe/Au人工規則合金

- $[Fe(1ML)/Au(1ML)]_N$ is a $L1_0$ type ordered alloy that does not exist in nature (Peritechtic system)
  $[Fe(1ML)/Au(1ML)]_N$は天然には存在しない$L1_0$型の規則合金である。
- At interfaces in Fe/Au, $L1_0$ type Fe(1ML)/Au(1ML) exists
  $[Fe(x\mathrm{ML})/Au(x\mathrm{ML})]_N$においても、Fe層とAu層の界面には$L1_0$型Fe(1ML)/Au(1ML)が存在
- New band structure appears due to hybridization
  FeとAuの間には電子の混成が生じ、新しいバンド構造が出現している。

Atomic arrangement in a unit cell of Fe(1ML)/Au(1ML) with a $L1_0$ structure

Fe(1ML)/Au(1ML)人工規則合金の結晶構造

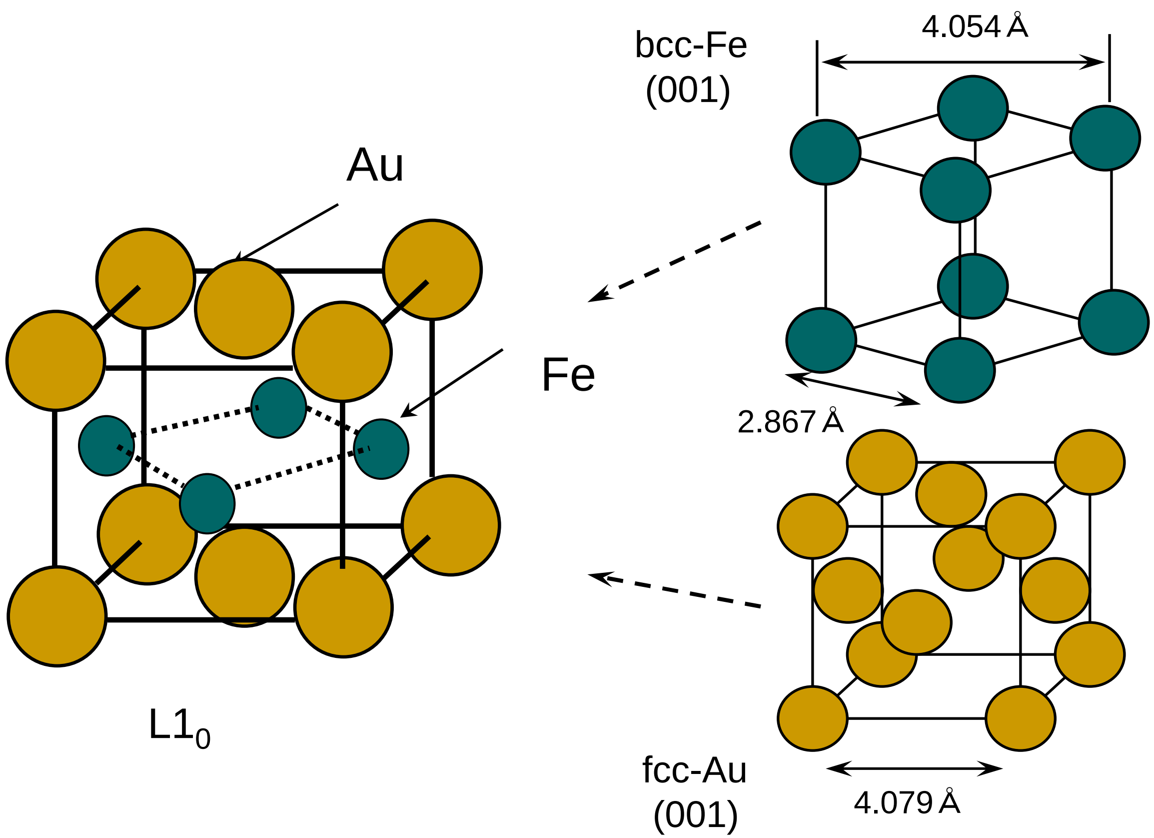

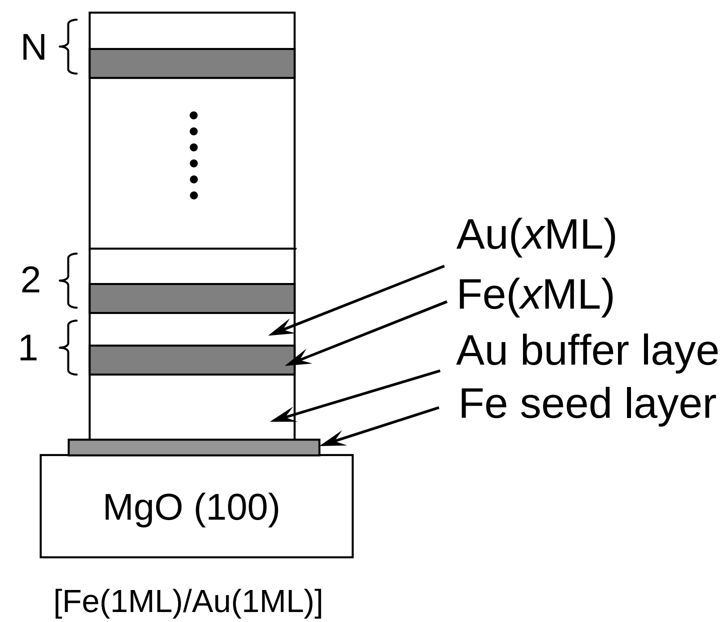

Schematic structure for the Fe/Au superlattice

整数･非整数層厚をもつFe/Au人工格子

Superlattices :〔Fe(xML)/Au(xML)〕$_N$ with integer and non-integer layer thickness

x=1, 1.25, 1.5, 1.75,1, 2.25, 2.5, 2.75, 3.25, 3.5, 3.75, 4, 6, 8, 10, 15

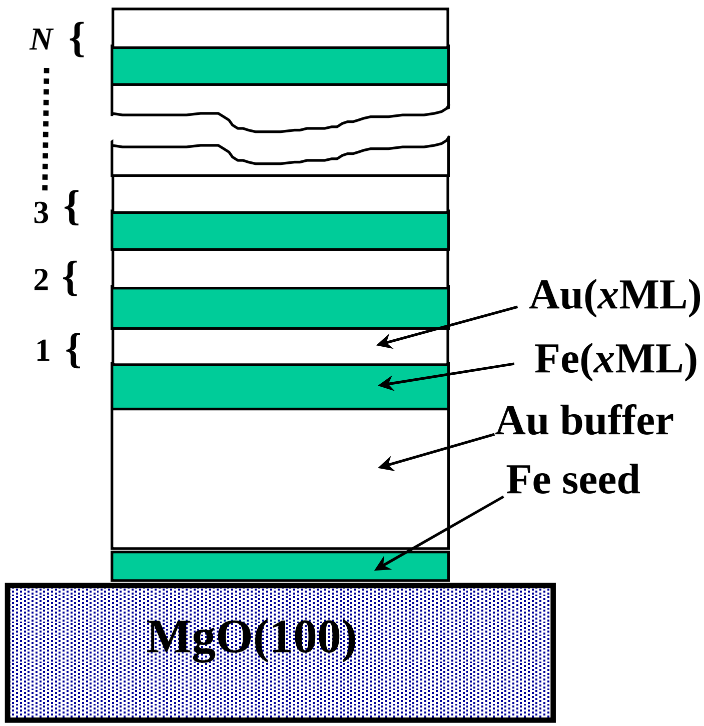

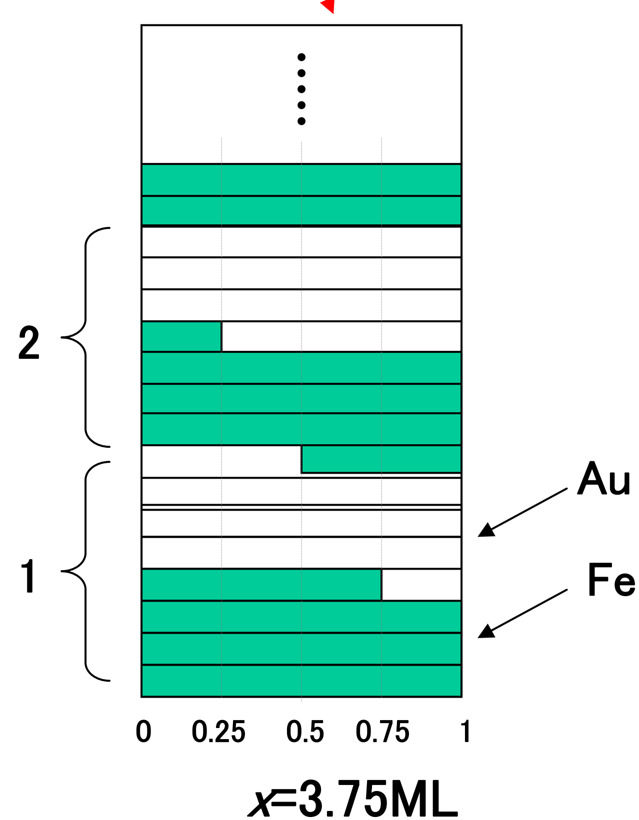

Retardation modulation technique
光学遅延変調法（円偏光変調法）

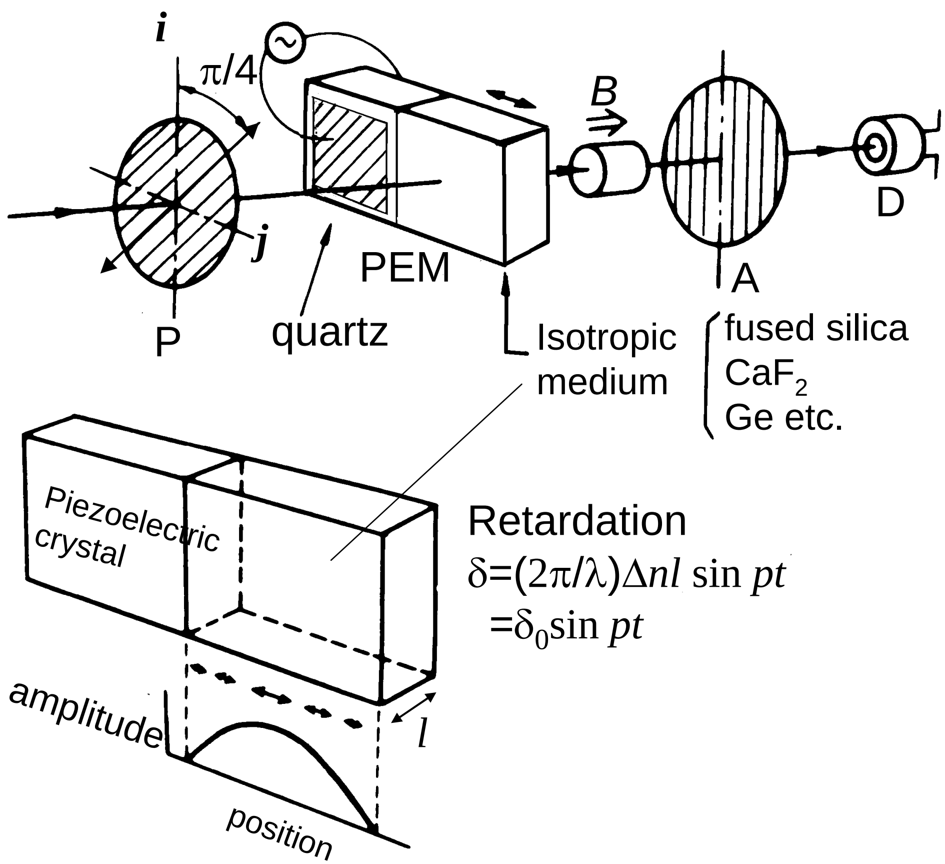

Retardation

$\delta=(2\pi/\lambda)\Delta nl\ \sin pt$

$=\delta_0 \sin pt$

Magneto-optical spectrometer system
磁気光学スペクトル測定系

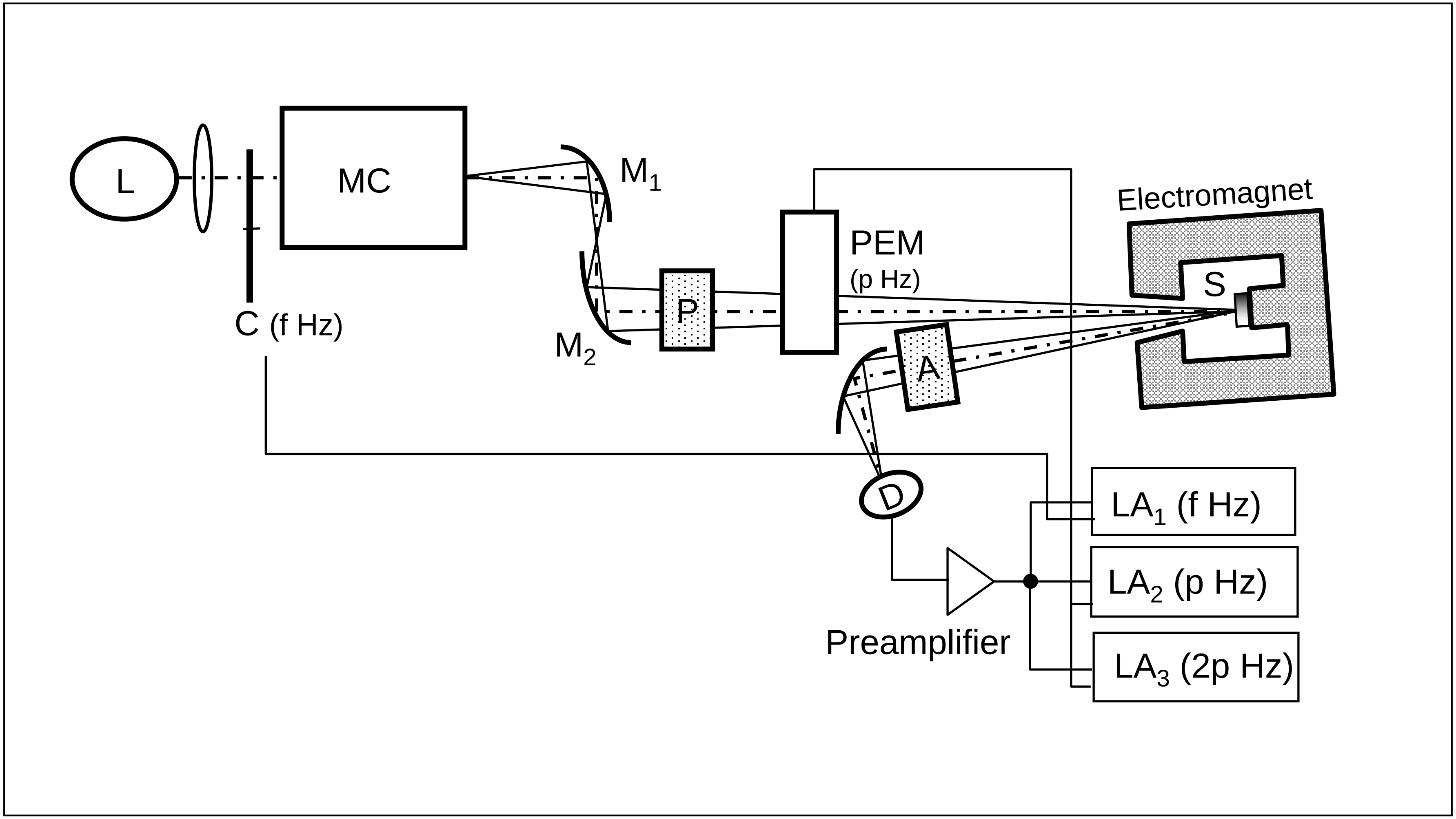

Magneto-optical Kerr spectra in Fe/Au superlattices

Fe(xML)/Au(xML)人工格子における磁気光学カー回転角のスペクトル

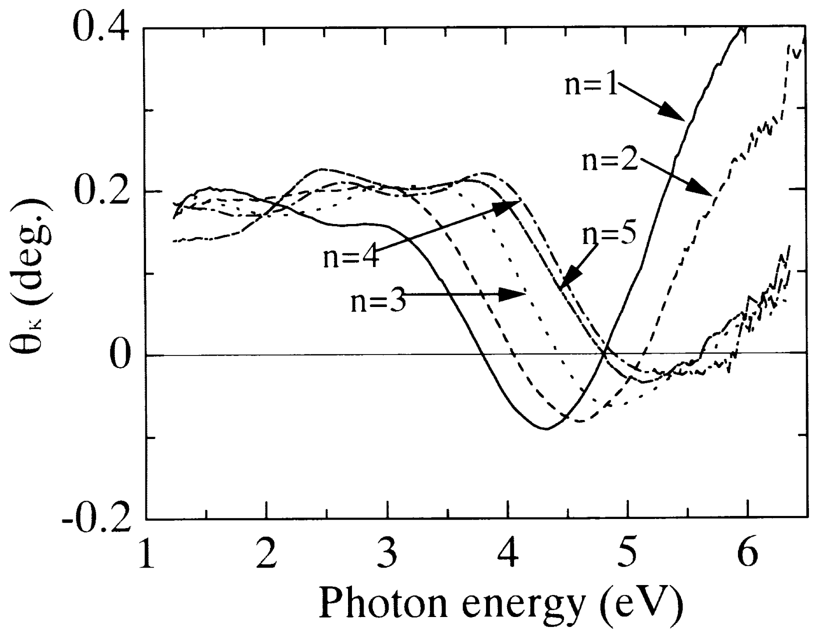

x=1～5

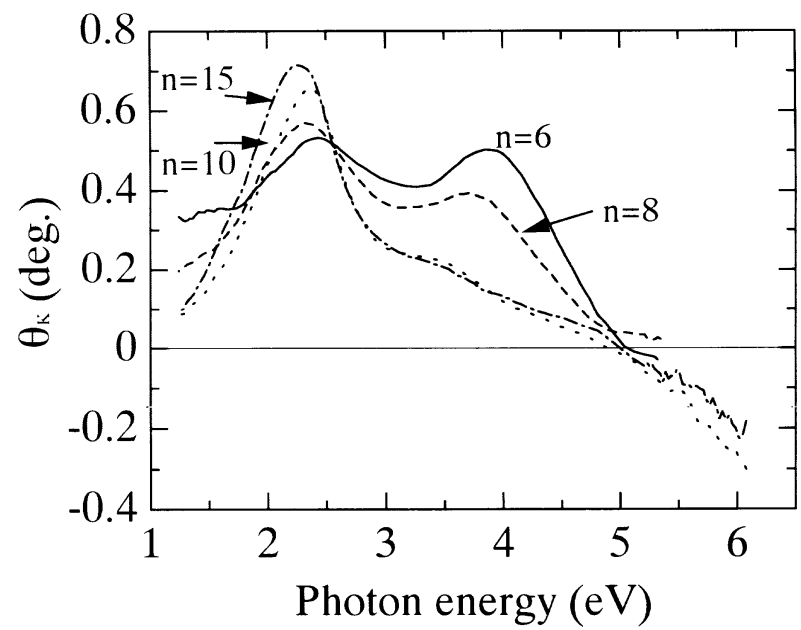

x=6～15

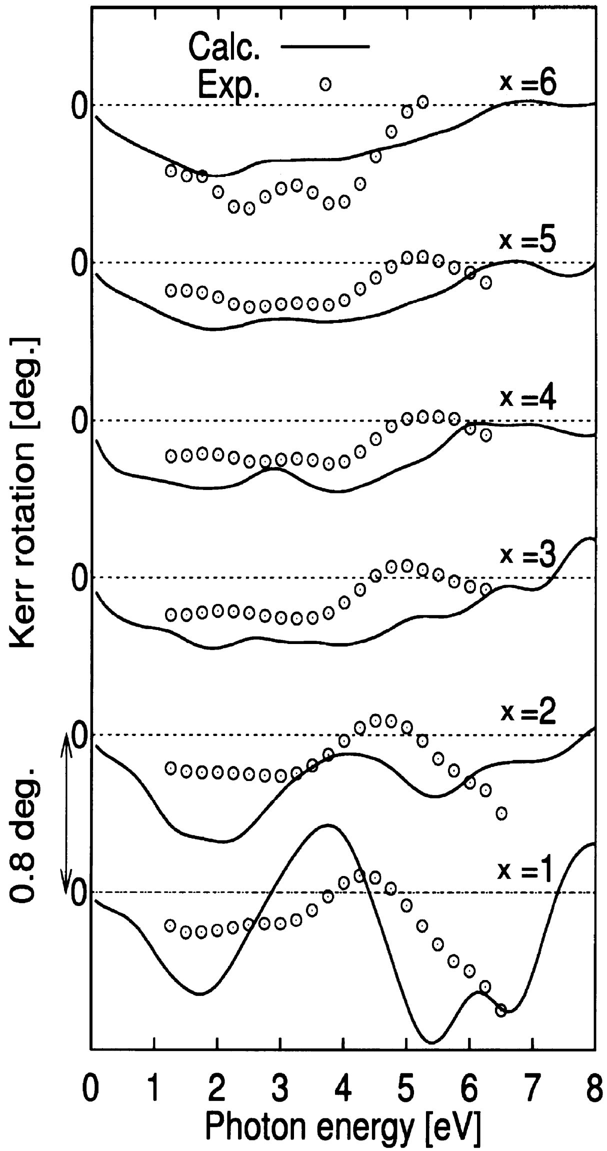

Calculated Kerr spectra in Fe/Au superlattices using ab-initio band calculation

第１原理バンド計算によるFe(xML)/Au(xML)人工格子の磁気光学スペクトル（山口による）

The structure around 4eV can be assigned to Au(5d↓) to Fe(3d↓) transition

4eV付近に見られる構造は、Auの5d↓バンドからAuの5f↓バンドへの遷移である。Auの5f↓バンドはFeの3d↓バンドと強く混成しており、実質的にはAu(5d↓)→Fe(3d↓)遷移と見なせる。

Peak position of Kerr rotation vs. modulation period

Fe/Au人工格子の磁気光学スペクトルのピーク位置の変調周期に対するプロット。

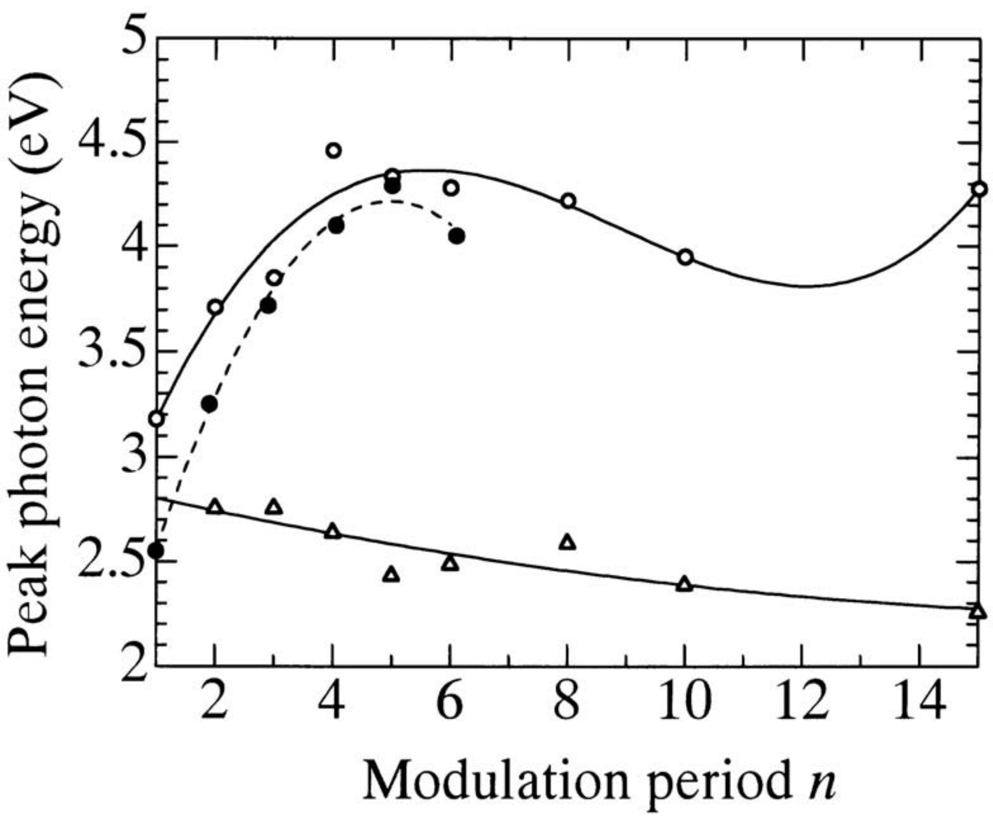

Dotted curve denotes the peak position in magneto-optical spectra of Au/Fe/Au ultrathin trilayer

点線は、超薄膜における量子閉じ込めピークの変調周期依存性。

MSHG study of magnetism for surfaces and interfaces

→ **The effect is quite sensitive to surfaces and interfaces where inversion symmetry is broken.**

↓

Magnetic second harmonic generation (MSHG) has been applied to study of magnetic thin film and multilayer

Scheme

Fe/Au superlattices with a modulation of mono-atomic layers

↓

MSHG technique was applied to Fe/Au superlattices

SHG

- For weak incident laser field E(ω) :

$$P_i^{(1)} = \chi_{ij}^{(1)} \varepsilon_0 E_j$$

linear response

- For strong incident laser field E(ω) :

$$P_i = \varepsilon_0 (\chi_{ij}^{(1)} E_j + \chi_{ijk}^{(2)} E_j E_k + \chi_{ijkl}^{(3)} E_j E_k E_l + \cdots)$$

Nonlinear response

Third rank tensor is not allowed in *centrosymmetric* materials.

- Nonlinear polarization *$P^{(2)}$ for incident field of* $\mathbf{E} = \mathbf{E}_0 \sin \omega t$

$$P^{(2)} = \varepsilon_0 \chi^{(2)} \frac{E_0}{2} + \varepsilon_0 \chi^{(1)} E_0 \sin \omega t - \varepsilon_0 \chi^{(2)} \frac{E_0^2}{2} \cos 2\omega t + \cdots$$

Second harmonic generation (SHG)

Nonlinear magneto-optical effect measurement system

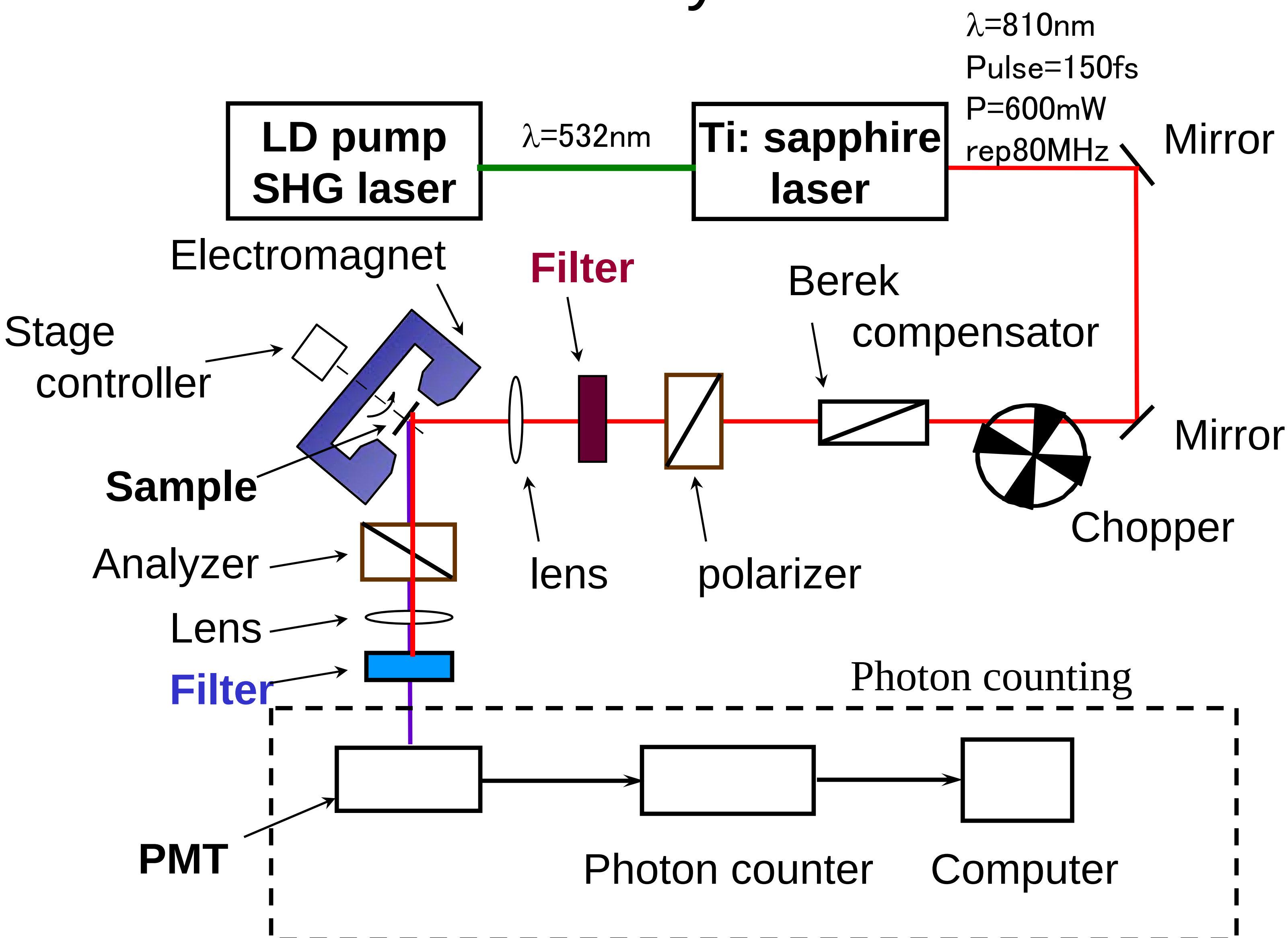

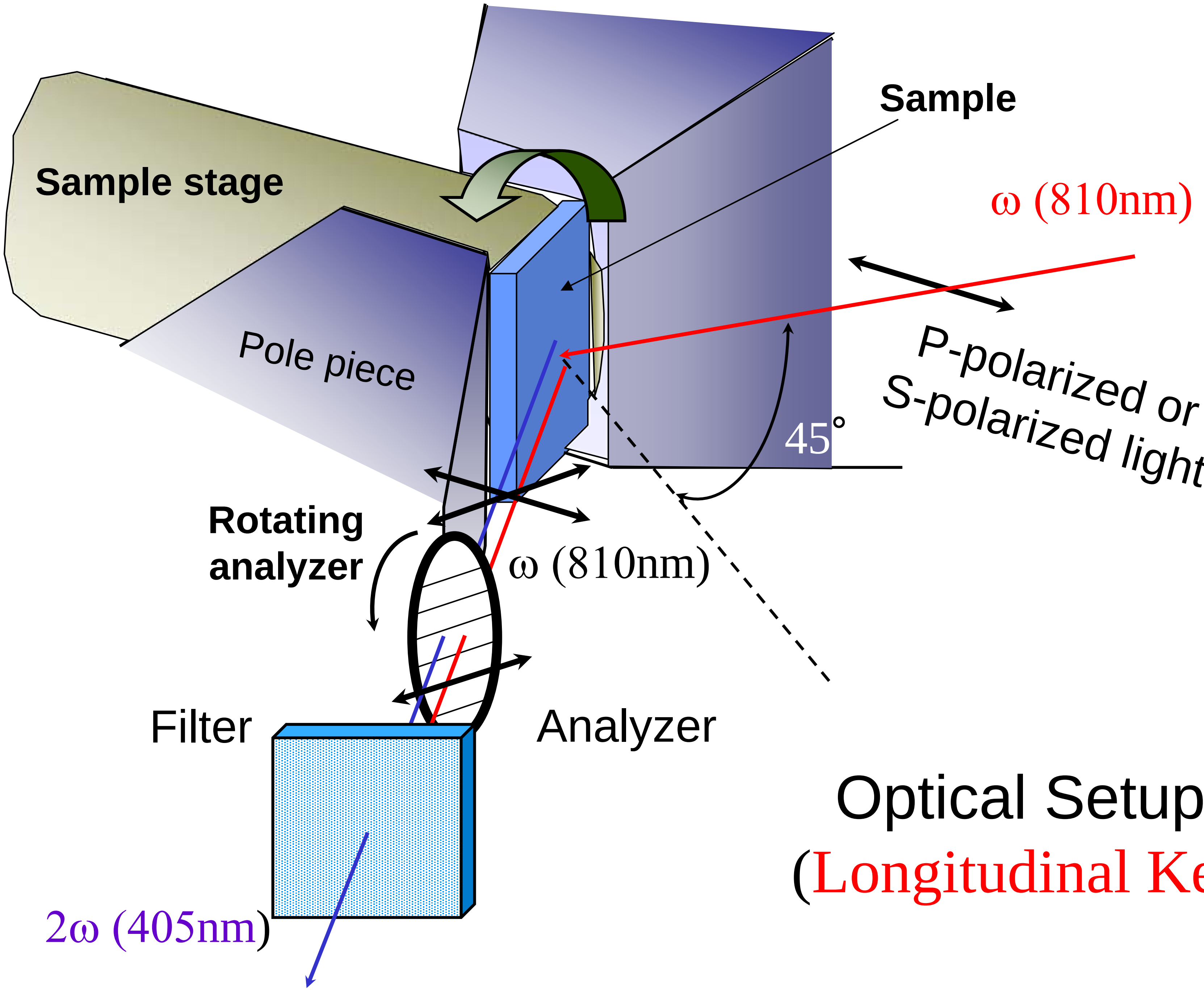

Optical Setups
(Longitudinal Kerr)

Result

Analyzer angle-dependence of MSHG

MSHGの検光子角依存性

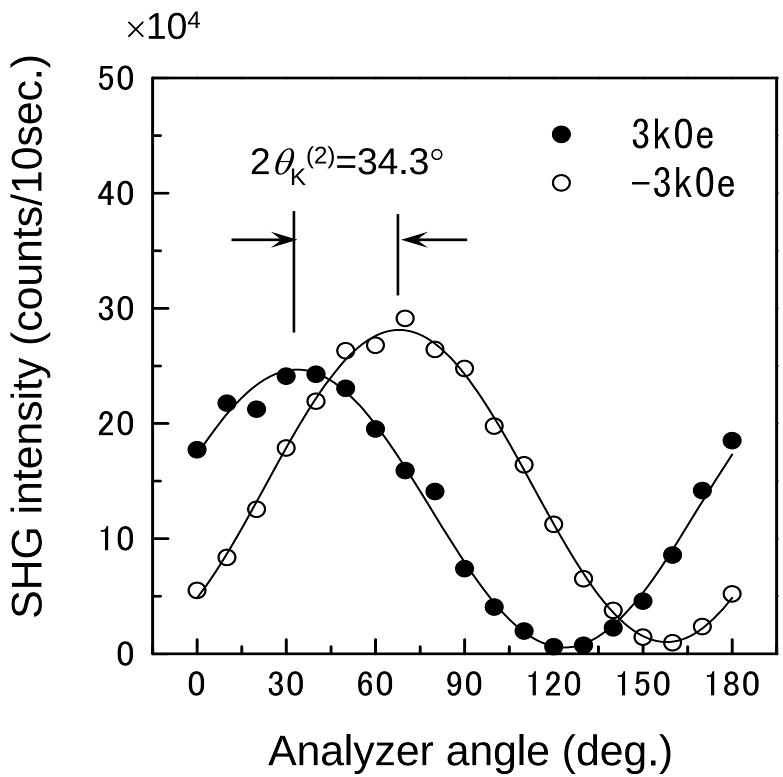

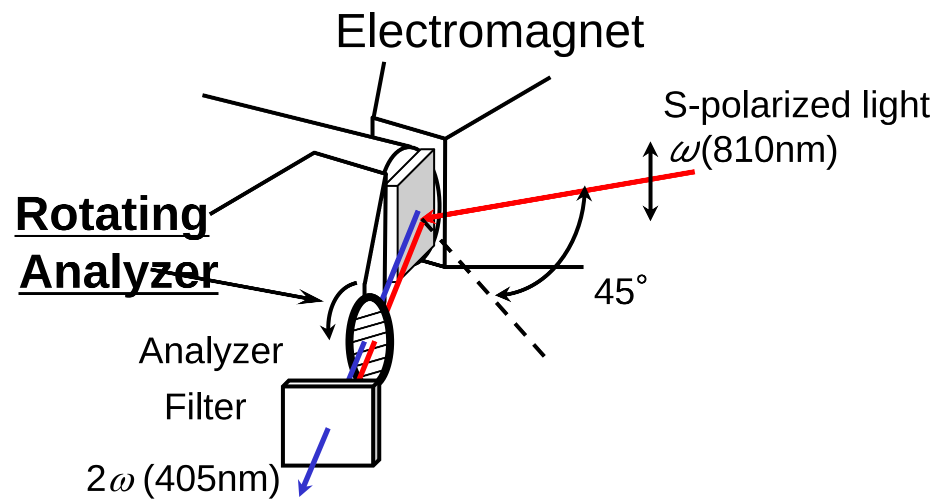

The curves show a shift for two opposite directions of magnetic field

$$\eta_K^{(2)} = \frac{1}{2}\left[\tan^{-1}\left(\frac{I_{MAX}(+)}{I_{MIN}(+)}\right) - \tan^{-1}\left(\frac{I_{MAX}(-)}{I_{MIN}(-)}\right)\right]$$

Analyzer angle-dependence for
[Fe(3.5ML)/Au(3.5ML)] superlattice (Sin)

Nonlinear Kerr rotation & ellipticity

$\theta_K^{(2)}$= 17.2 °

$\eta_K^{(2)}$=3°

Result

Nonlinear Kerr rotation : $\Delta\phi$

$\Delta\phi = 2.74^\circ$

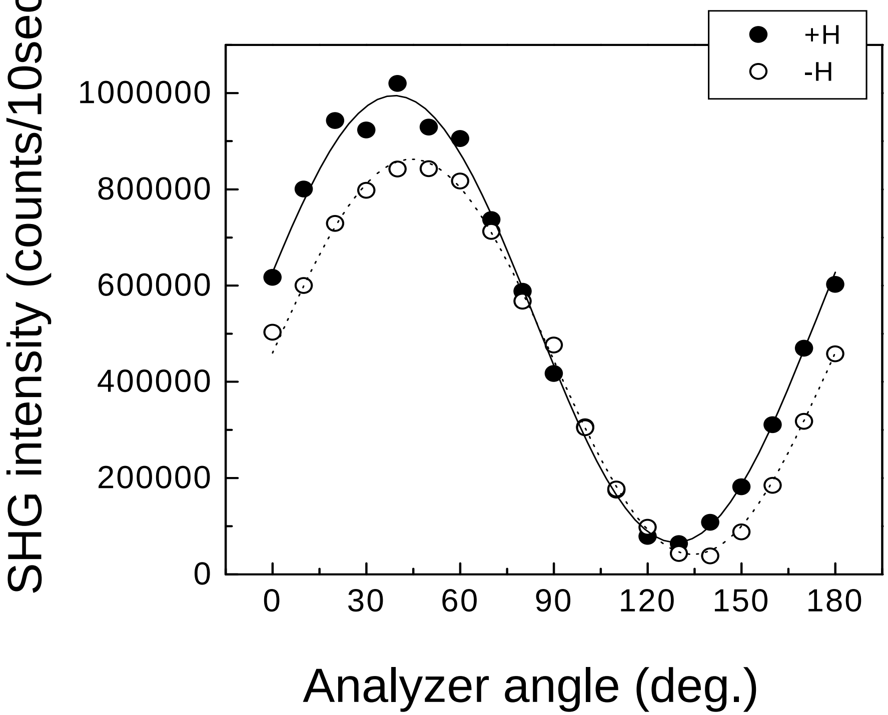

(a) Fe(1ML)/Au(1ML) Pin

$\Delta\phi = 31.1^\circ$

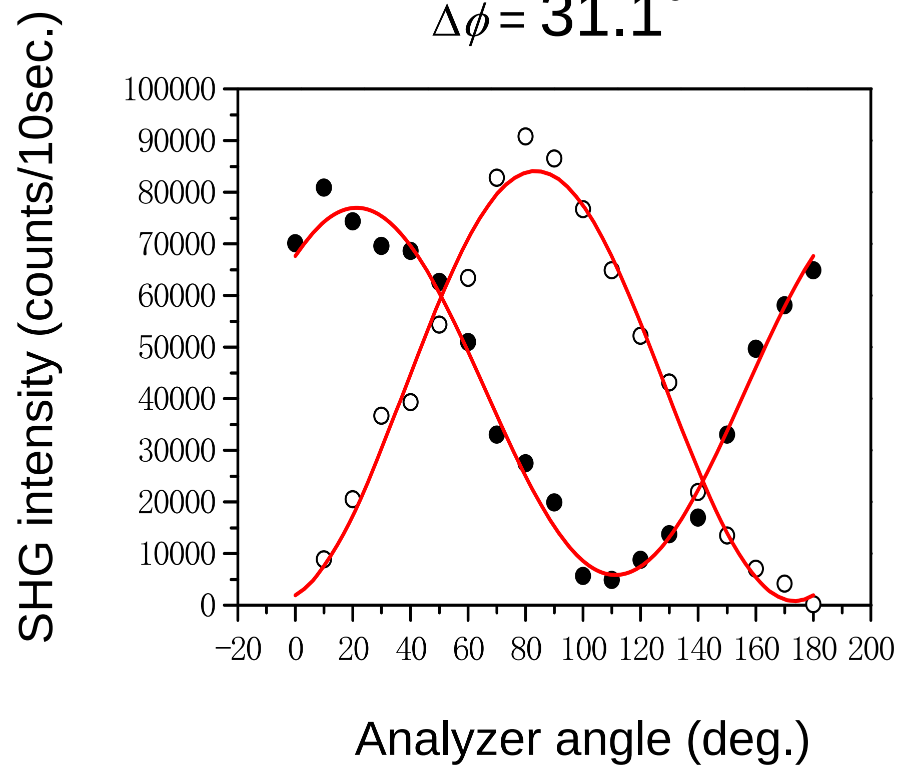

(b) Fe(1.75ML)/Au(1.75ML) Sin

Analyzer angle dependence

Azimuthal angle-dependence of MSHG

- Linear optical response (λ=810nm)
  The isotropic response for the azimuthal angle
- Nonlinear optical response (λ=405nm)
  The 4-fold symmetry pattern
  Azimuthal pattern show 45°-rotation by reversing the magnetic field

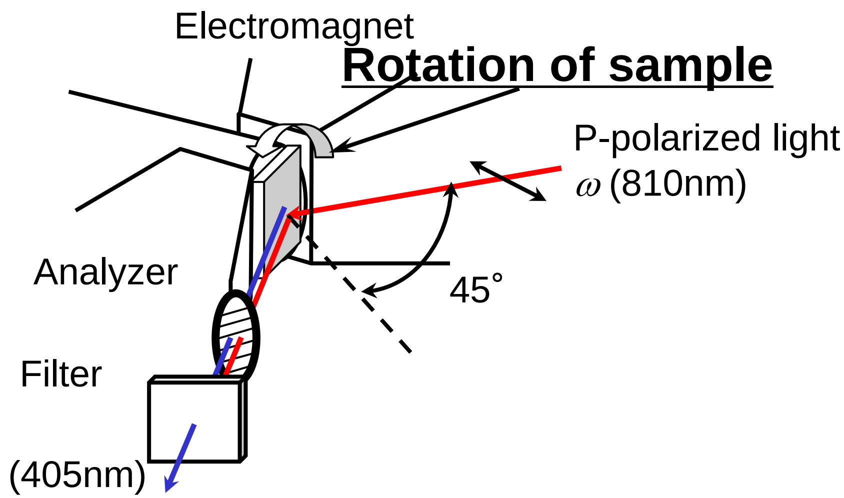

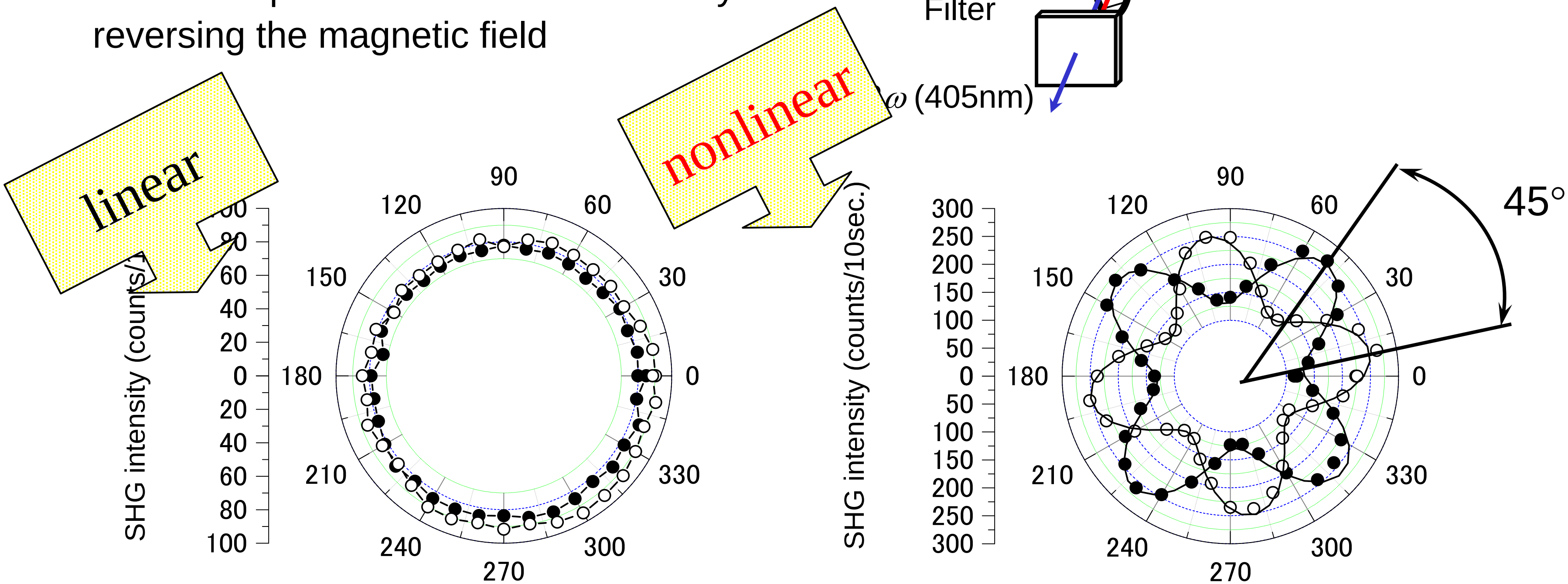

(a) Linear (810nm) (b) SHG (405nm)

Azimthal angle-dependence of MSHG intensity for [Fe(3.75ML)/Au(3.75ML)] superlattice. (P_{in} P_{out})

Azimuthal dependence of MSHG in fractional superlattices

Pin-Pout

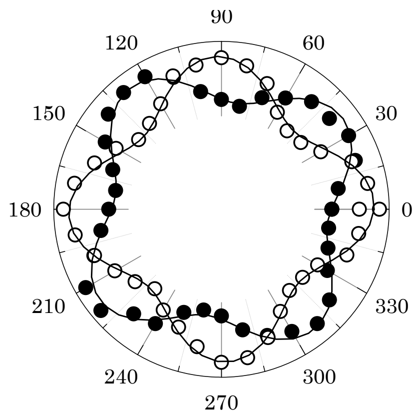

Fe(3.5ML)/Au(3.5ML)

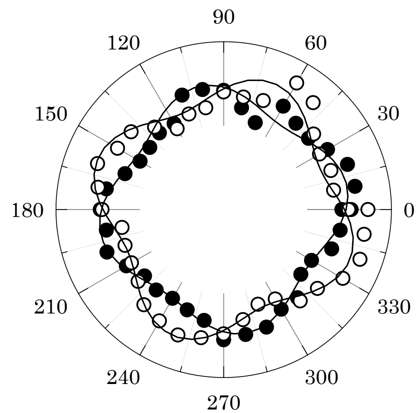

Fe(2.75ML)/Au(2.75ML)

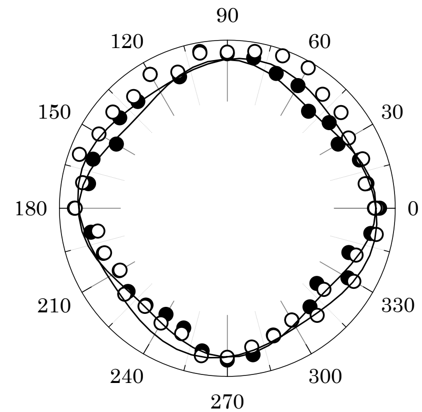

Fe(2.25ML)/Au(2.25ML)

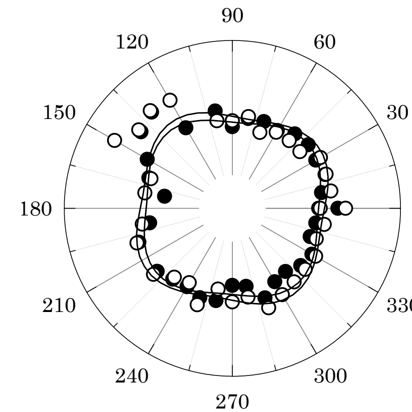

Fe(1.5ML)/Au(1.5ML)

Sin-Sout

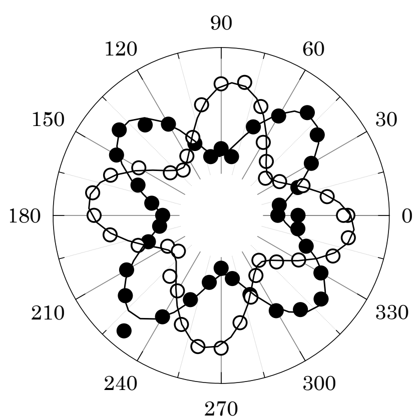

Fe(3.5ML)/Au(3.5ML)

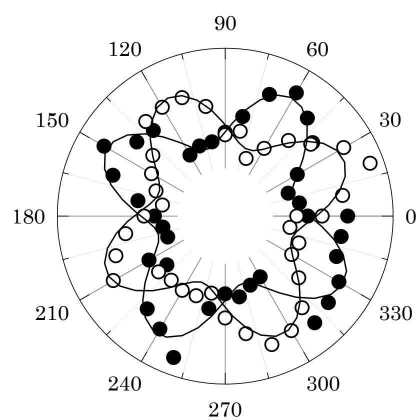

Fe(2.75ML)/Au(2.75ML)

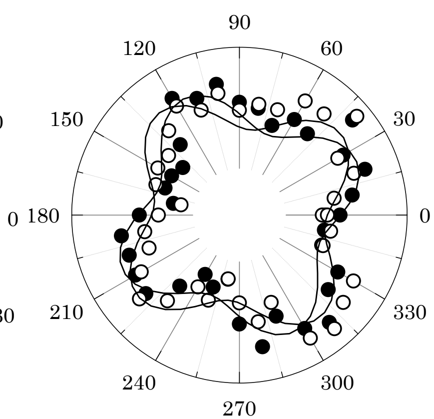

Fe(2.25ML)/Au(2.25ML)

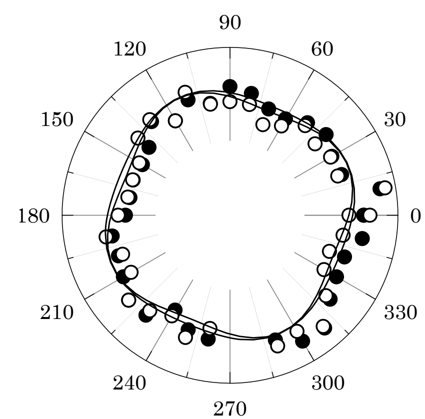

Fe(1.25ML)/Au(1.25ML)

Discussion

The equation of the azimuthal angle-dependence by the theoretical analysis

$$P_i^{(2)}(2\omega) = \underline{\chi_{ijk}^{(D)} E_j(\omega) E_k(\omega)} + \underline{\chi_{ijkl}^{(Q)} E_j(\omega) \nabla_k E_l(\omega)}$$

$$\underline{+ \mathrm{X}_{ijkL}^{(S)} E_j(\omega) E_l(\omega) M_L}$$

A: Surface nonmagnetic term

- The electric dipole origin give rise to isotropic signal.

B: Bulk nonmagnetic term

- The quadrupole origin causes an anisotropic contribution for four rank tensor.

C: Surface magnetic term

- The time reversal symmetry is lifted by magnetization
- Mirror symmetry operations should be supplemented with an additional reversion of M.

Surface non-magnetic term

- SHG response causes an isotropic contribution only.

Bulk non-magnetic term

$$P_i(2\omega) = \chi^{(D)}_{ijk} E_j(\omega) E_k(\omega) + \chi^{(Q)}_{ijkl} E_j(\omega) \nabla_l E_k(\omega)$$

- For crystallographic contribution the electric quadrupole should be introduced to get four rank tensor.

⇨ SHG response causes an anisotropic contribution (parameter B).

Surface magnetization induced term

$$\chi^{S}_{ijk}(M) = \chi^{S}_{ijk}(0) + X^{S}_{ijkL} M_L$$

- The surface magnetic response comes from the electric dipole term expanded by magnetization and contributes to the parameter C.

Calculated azimuthal angle dependence of SHG and MSHG signals

input-output polarization	surface non-magnetic	bulk non-mangetic	surface magnetization-induced	sum
S_{in}-S_{out}	0	$\lvert B\sin 4\phi\rvert^2$	$\lvert \pm A_{ss} \pm C\cos 4\phi\rvert^2$	$\lvert \pm \boldsymbol{A}_{ss} + \boldsymbol{B}\sin 4\phi \pm \boldsymbol{C}\sin 4\phi\rvert^2$
S_{in}-P_{out}	$\lvert A'_{sp}\rvert^2$	$\lvert A_{sp} - B\cos 4\phi\rvert^2$	$\lvert \pm C\sin 4\phi\rvert^2$	$\lvert \boldsymbol{A}_{sp} - \boldsymbol{B}\cos 4\phi \pm \boldsymbol{C}\sin 4\phi\rvert^2$
P_{in}-S_{out}	0	$\lvert -B\sin 4\phi\rvert^2$	$\lvert \pm A_{ps} \mp C\cos 4\phi\rvert^2$	$\lvert \pm \boldsymbol{A}_{ps} - \boldsymbol{B}\sin 4\phi + \boldsymbol{C}\cos 4\phi\rvert^2$
P_{in}-P_{out}	$\lvert A'_{pp}\rvert^2$	$\lvert A_{pp} + B\cos 4\phi\rvert^2$	$\lvert \mp C\sin 4\phi\rvert^2$	$\lvert \boldsymbol{A}_{pp} + \boldsymbol{B}\cos 4\phi \mp \boldsymbol{C}\sin 4\phi\rvert^2$

Kerr rotation calculated from parameters Axx,B,C $\Theta_K^{(2)} = (\psi_+ - \psi_-)/2$

S_{in} $$\tan 2\psi_\pm = \frac{2(A_{SP} - B\cos 4\phi \pm C\sin 4\phi)(\pm A_{SS} + B\sin 4\phi \pm C\cos 4\phi)}{(A_{SP} - B\cos 4\phi \pm C\sin 4\phi)^2 - (\pm A_{SS} + B\sin 4\phi \pm C\cos 4\phi)^2}$$

P_{in} $$\tan 2\psi_\pm = \frac{2(A_{PP} + B\cos 4\phi \mp C\sin 4\phi)(\pm A_{PS} - B\sin 4\phi \pm C\cos 4\phi)}{(A_{PP} + B\cos 4\phi \mp C\sin 4\phi)^2 - (\pm A_{PS} - B\sin 4\phi \pm C\cos 4\phi)^2}$$

Calculated polar patterns of the azimuthal angle-dependence (Sin-Pout)

Without quadrupole term

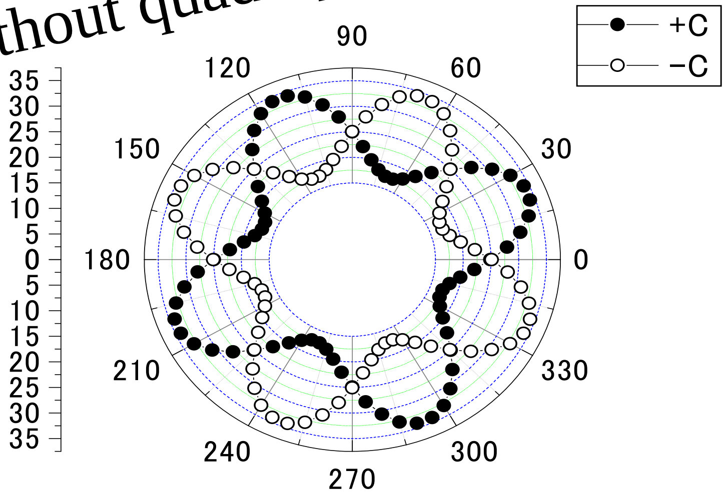

(a) A=5, B=0, C=0.85

With quadrupole term

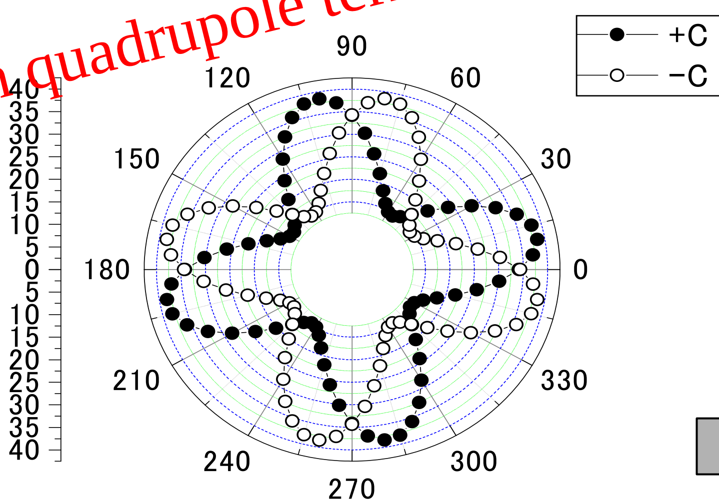

(b) A=5, B=0.85, C=0.85

The equation of the azimuthal angle-dependence by theoretical analysis

$$I^{SP} = \left| A^{SP} - B\cos 4\varphi \pm C\sin 4\varphi \right|^2$$

(a) A=5, B=0, C=0.85

- For B much smaller than C, the polar pattern shows 45° rotation for the magnetization reversal.

(b) A=5, B=0.85, C=0.85

- For B comparable C, the polar pattern undergo a smaller rotation.

The azimuthal pattern was interpreted in terms of combination of B and C.

Azimuthal angle-dependence of MSHG for a 「Fe(3.5ML)/Au(3.5ML)] superlattice (Sin-Pout, Sin-Sout configuration)

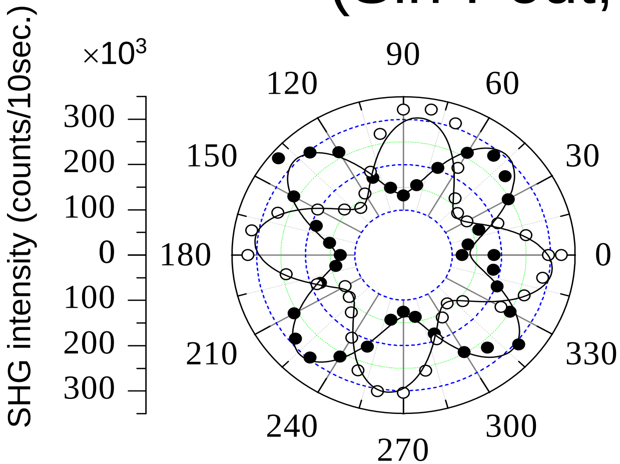

(a) Sin-Pout

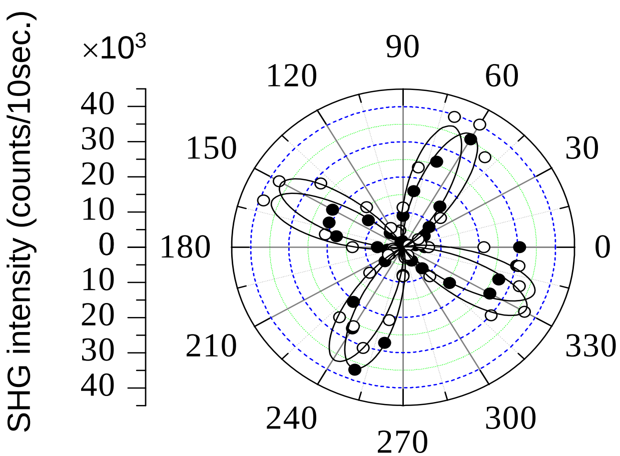

(b) Sin-Sout

The equation of the azimuthal angle-dependence by theoretical analysis

Sin-Pout

$$I^{SP} = \left| A^{SP} - \underline{\boldsymbol{B}}\cos 4\varphi \pm \underline{\boldsymbol{C}}\sin 4\varphi \right|^2$$

Sin-Sout

$$I^{SS} = \left| \pm A^{SS} \pm \underline{\boldsymbol{C}}\cos 4\varphi + \underline{\boldsymbol{B}}\sin 4\varphi \right|^2$$

A^{SP}(surface nonmagnetic term)	=	460
A^{SS}(surface nonmagnetic term)	=	100
B(bulk nonmagnetic term)	=	26
C(surface magnetic term)	=	-88

Calculated and experimental patterns :x=3.5

Dots：exp.
Solid curve：calc.

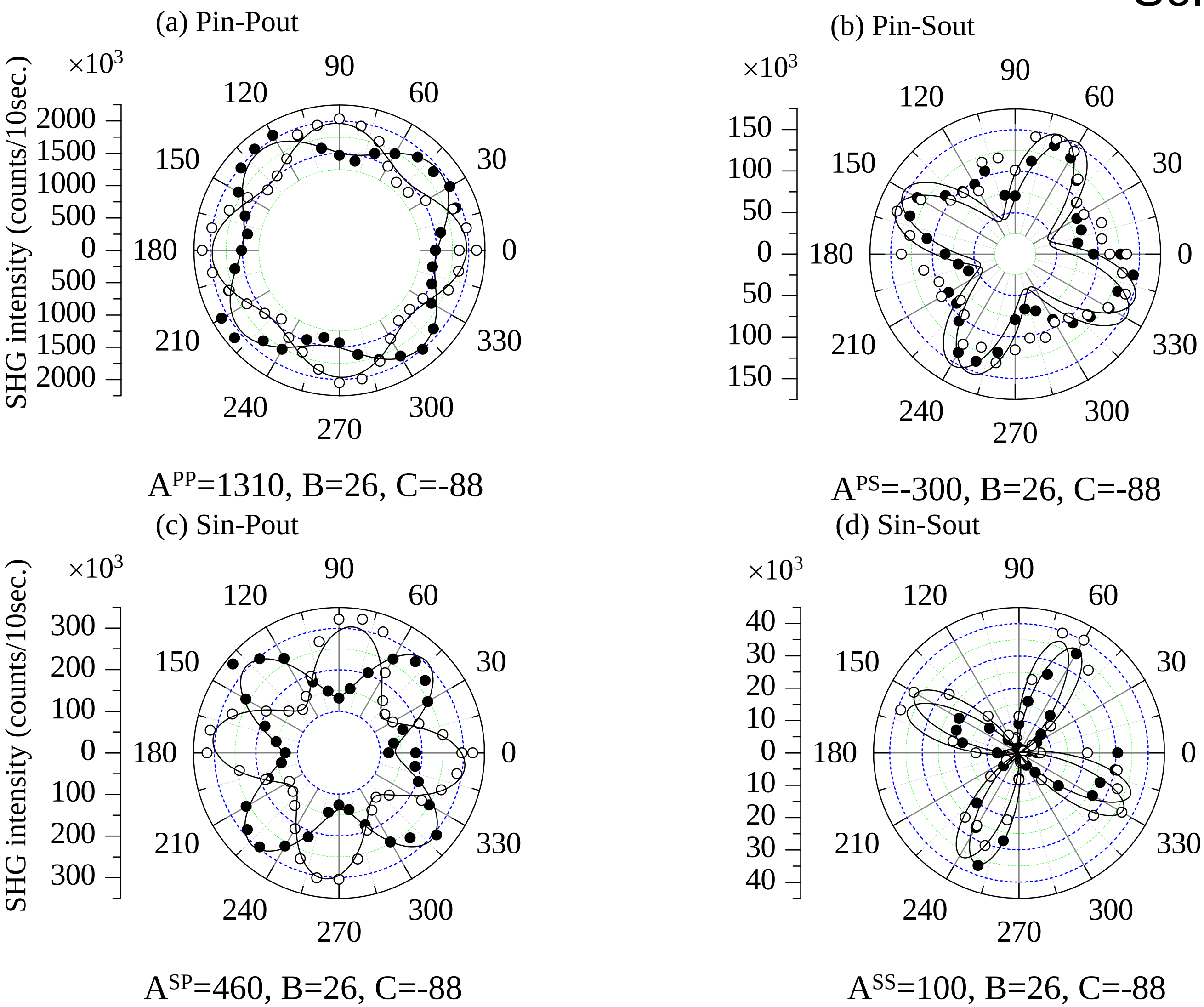

The fitting parameter of the azimuthal pattern (Sin-Pout)

$$I^{SP} = \left| A^{SP} - B\cos 4\varphi \pm C\sin 4\varphi \right|^2$$

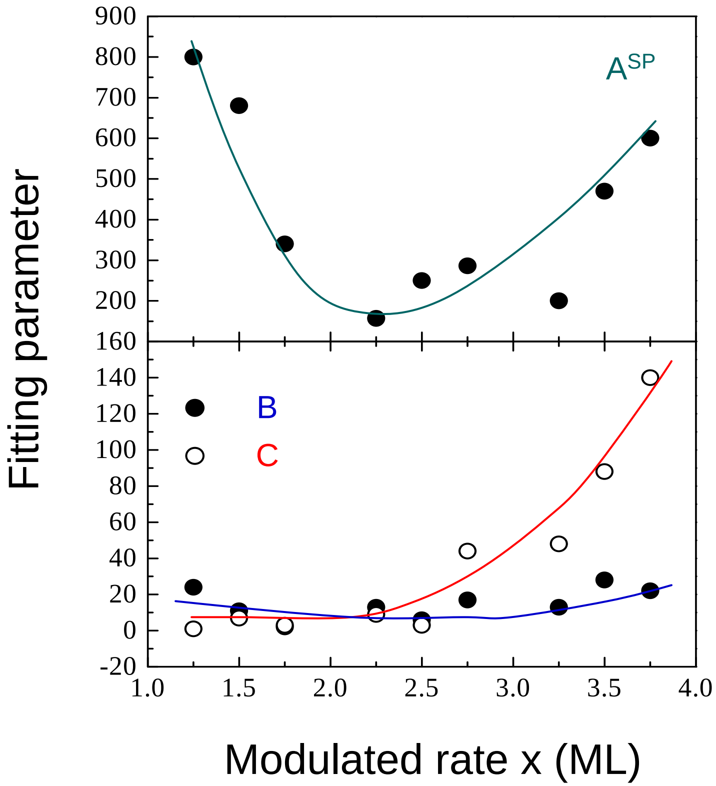

Fig. The fitting parameter of azimuthal angle-dependence for [Fe(xML)/Au(xML)] (1.25≤x≤3.75) superlattices.

Contribution of A^{SP} term

- Surface nonmagnetic term
- Dependence on focused beam power

Contribution of B term

- Bulk nonmagnetic term
- The parameter B is constant for the modulation x.

Contribution of C term

- Surface magnetic term
- Decrease of the parameter C for the azimuthal patern rotation

The modulation period-dependence of fitting parameters and nonlinear Kerr rotation angle and ellipticity in [Fe(xML)/Au(xML)] ($1 \leq x \leq 4$) superlattices.

Input polarization is (a)Pin and (b)Sin.

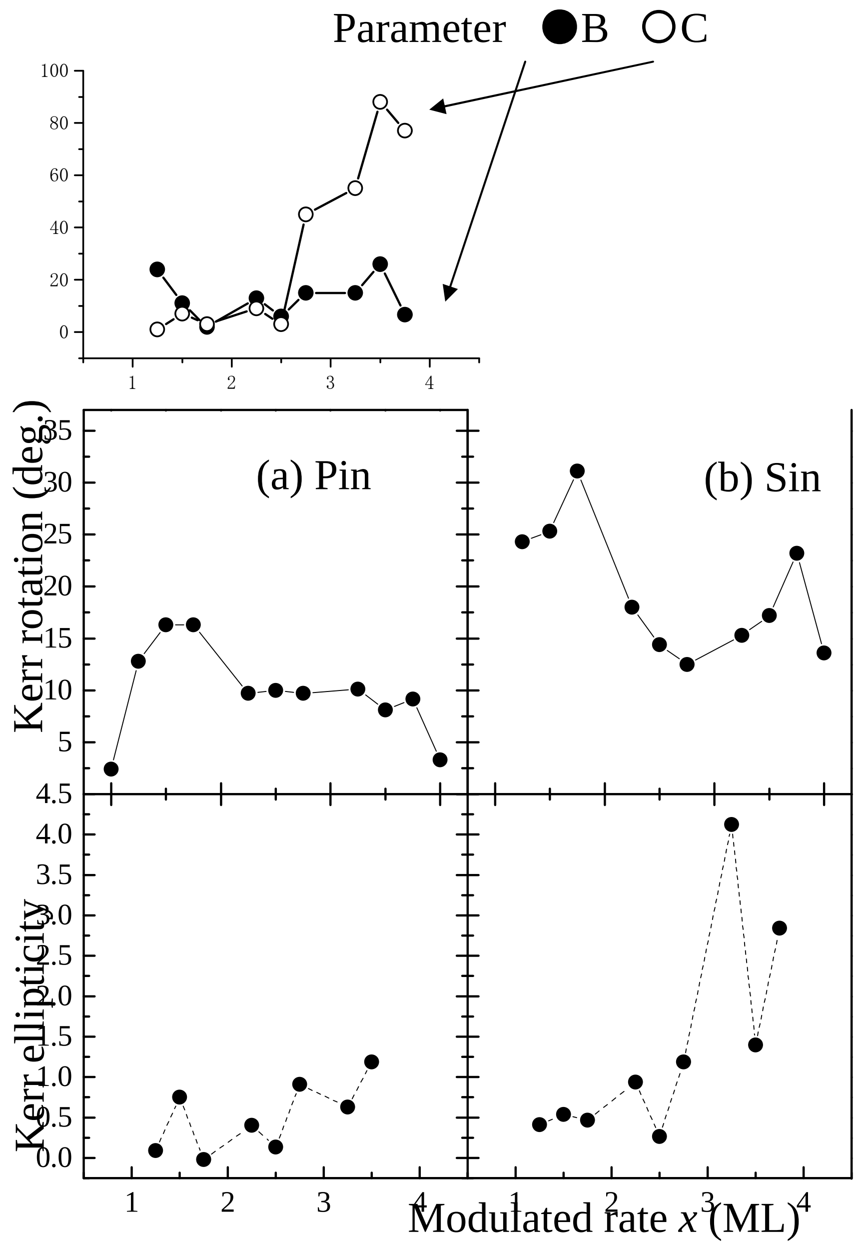

Nonlinear Kerr rotation

Nonlinear Kerr ellipticity

Azimuthal angle dependence of the MSHG intensity for the anlyzer angle

Fe(1.25ML)/Au(1.25ML)

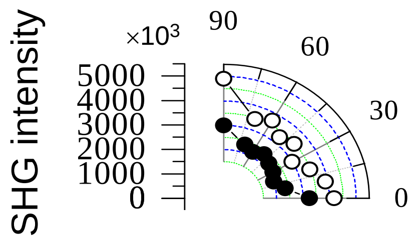

Analyzer angle = 30°

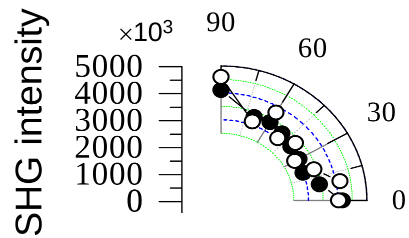

Analyzer angle = 60°
(Pin-Pout)

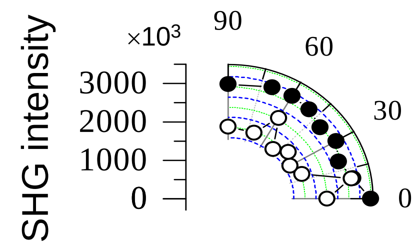

Analyzer angle = 90°

Fe(3.5ML)/Au(3.5ML)

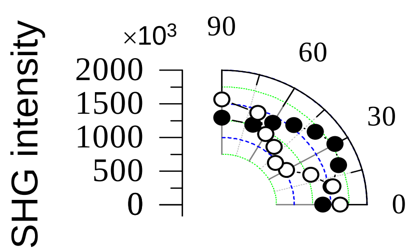

Analyzer angle = 30°

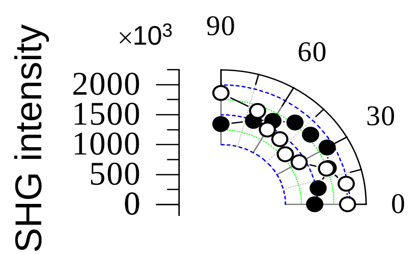

Analyzer angle = 60°
(Pin-Pout)

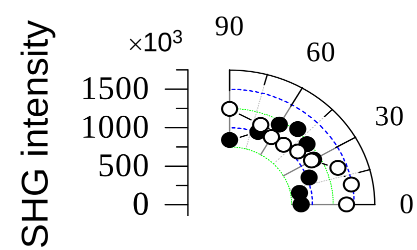

Analyzer angle = 90°

Experimental azimuthal angle-dependence of nonlinear Kerr rotation and ellipcity for a Fe(3.75ML)/Au(3.75ML) superlattice.(Sin)

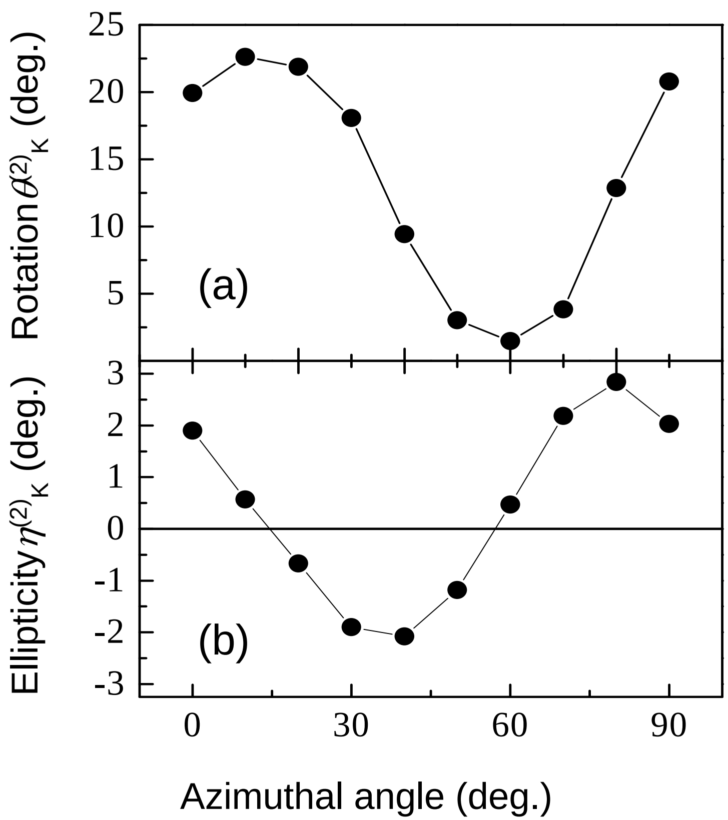

Fig. Calculated azimuthal angle-dependence of nonlinear Kerr rotation $\theta^{(2)}_K$ and ellipcity $\eta^{(2)}_K$ for a Fe(3.75ML)/Au(3.75ML) superlattice.

(a) Nonlinear Kerr rotation

- Azimuthal angle-dependence of nonlinear Kerr ellipticity is found to be sinusoidal.

(b) Nonlinear Kerr ellipticity

$$\eta_K^{(2)} = \frac{1}{2}\left[\tan^{-1}\left(\frac{I_{MAX}(+)}{I_{MIN}(+)}\right) - \tan^{-1}\left(\frac{I_{MAX}(-)}{I_{MIN}(-)}\right)\right]$$

I: Analyzer angle dependence of the MSHG intensity

- Azimuthal angle-dependence of nonlinear Kerr ellipticity showed 45°-shift compared to Kerr rotation.
- Ellipticity $\eta^{(2)}_K$ was about zero for the maximum $\theta^{(2)}_K$ and the minimum $\theta^{(2)}_K$.

Calculated azimuthal angle-dependence of nonlinear Kerr rotation and ellipcity for a Fe(3.75ML)/Au(3.75ML) superlattice.(Sin)

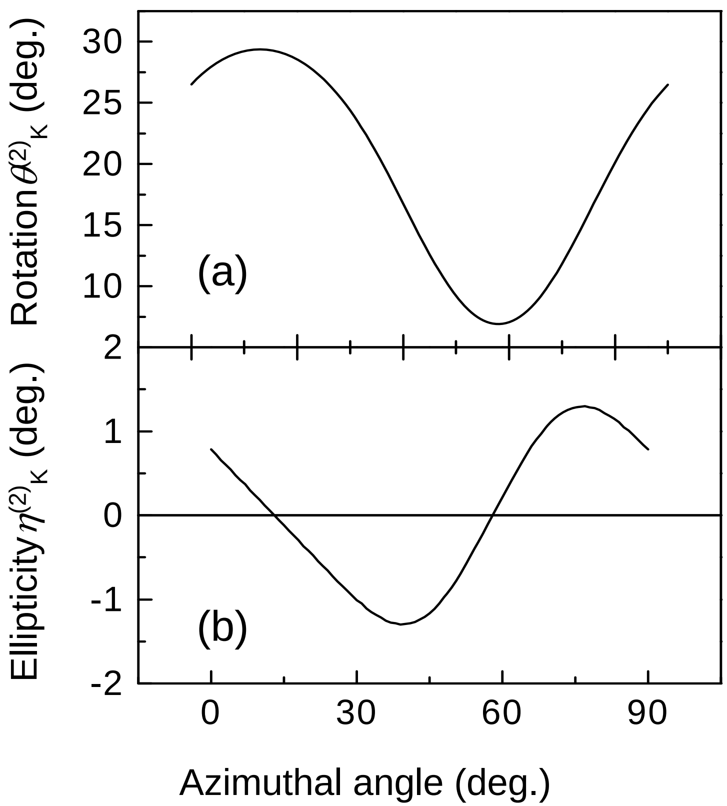

Fig. Experimental azimuthal angle-dependence of nonlinear Kerr rotation $\theta^{(2)}_K$ and ellipcity $\eta^{(2)}_K$ for a Fe(3.75ML)/Au(3.75ML) superlattice.

(a) Nonlinear Kerr rotation $\theta^{(2)}_K$

$$\tan\psi_{\pm} = \frac{2\left(A^{SP} - B\cos 4\varphi \pm C\sin 4\varphi\right)\left(\pm A^{SS} + B\sin 4\varphi \pm C\cos 4\varphi\right)}{\left(A^{SP} - B\cos 4\varphi \pm C\sin 4\varphi\right)^2 - \left(\pm A^{SS} + B\sin 4\varphi \pm C\cos 4\varphi\right)^2}$$

$$\Rightarrow \quad \theta_K^{(2)} = \frac{\psi_+ - \psi_-}{2}$$

(b) Nonlinear Kerr ellipticity $\eta^{(2)}_K$

$$I^{Sin}(\theta) = |P^{SP}\cos\theta + P^{SS}\sin\theta|^2$$

I: Analyzer angle-dependence of MSHG intensity for Pin configulation.

$$\Rightarrow \quad \eta_K^{(2)} = \frac{1}{2}\left[\tan^{-1}\left(\frac{I_{MAX}(+)}{I_{MIN}(+)}\right) - \tan^{-1}\left(\frac{I_{MAX}(-)}{I_{MIN}(-)}\right)\right]$$

Calculated and experimental pattern of Nonlinear Kerr rotation and ellipticity

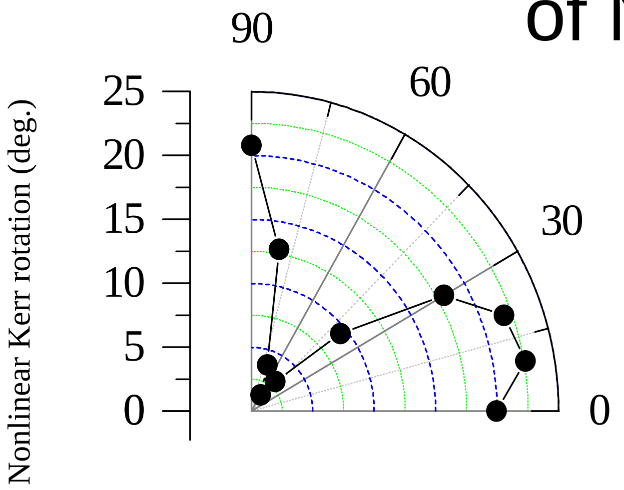

(a) Experimental pattern (Sin)

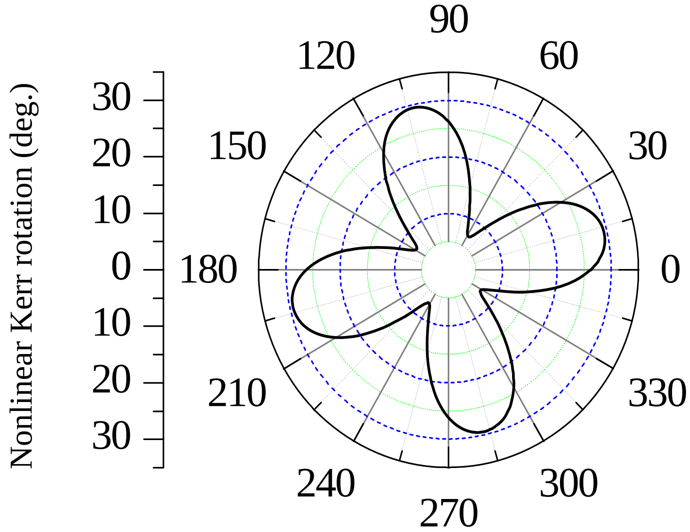

(b) Calculated pattern (Sin)

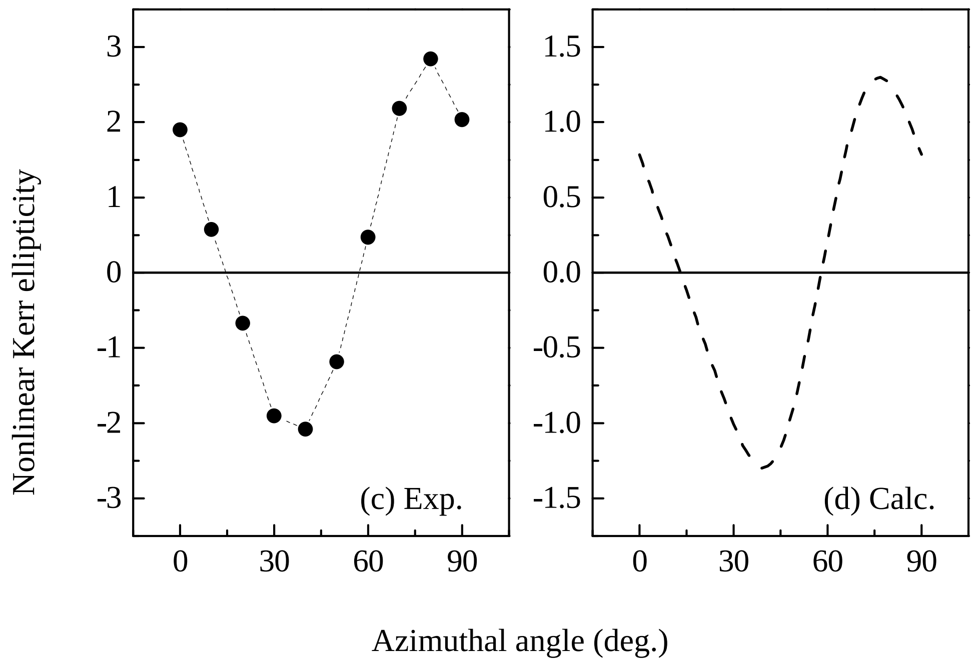

The azimuthal angle-dependences of nonlinear Kerr rotation angle and ellipticity
in [Fe(3.75ML)Au(3.75ML)]

Experimental and calculated patterns of Kerr rotation angle

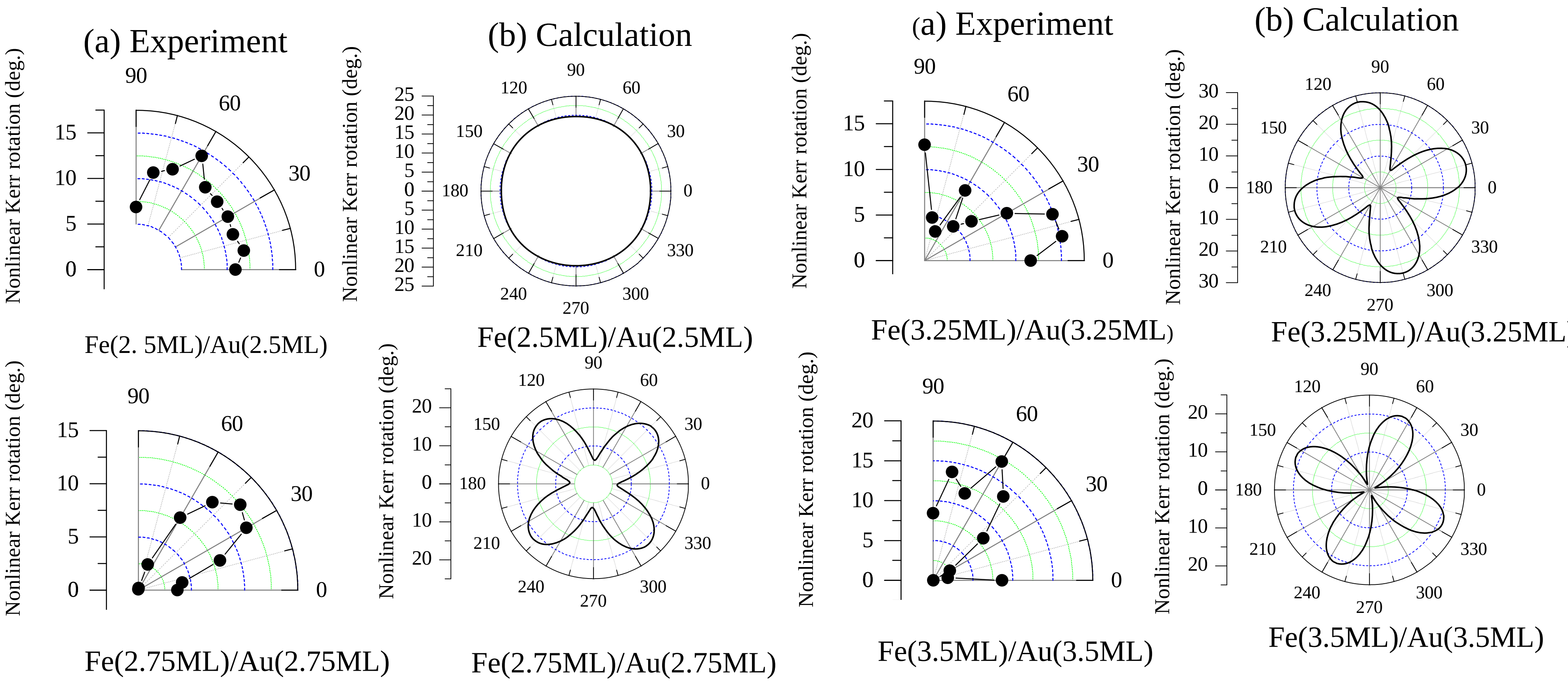

Sin configuration: (a) Experimental data,

(b) Calculated using *parameters determined by fitting to the azimuth patterns*

Nonlinear Kerr rotation angle of [Fe(xML)/Au(xML)] (1.25≤x≤3.75) superlattices (Sin)

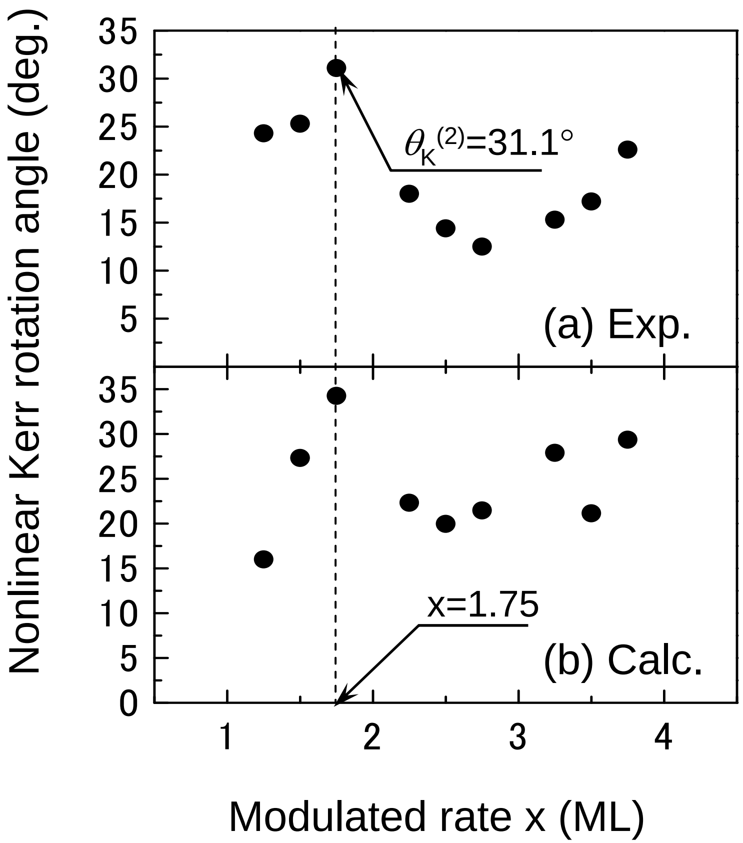

Fig. Nonlinear Kerr rotation angle of [Fe(xML)/Au(xML)] (1.25≤x≤3.75) superlattices [(a)Calculation, (b)Experiment]

Calculation and experimental result

Calculated nonlinear Kerr rotation angle $\theta_K^{(2)}$ using the fitting parameter A^{SP}, A^{SS}, B, C of the azimuthal pattern
(The maximum $\theta_K^{(2)}$ was selected for azimuth angle)

- The experimental maximum $\theta_K^{(2)}$ for x=1.75 superlattice was 31.1°.
- The calculated $\theta_K^{(2)}$ reproduced the muximum $\theta_K^{(2)}$ for x=1.75 superlattice.

The nonlinear Kerr rotation was explained by theoretical analysis.

Linear magneto-optical spectra in Co/Ru superlattice

Co(5ML)/Ru(5ML)の線形磁気光学スペクトルの実験値とバンド計算による理論値

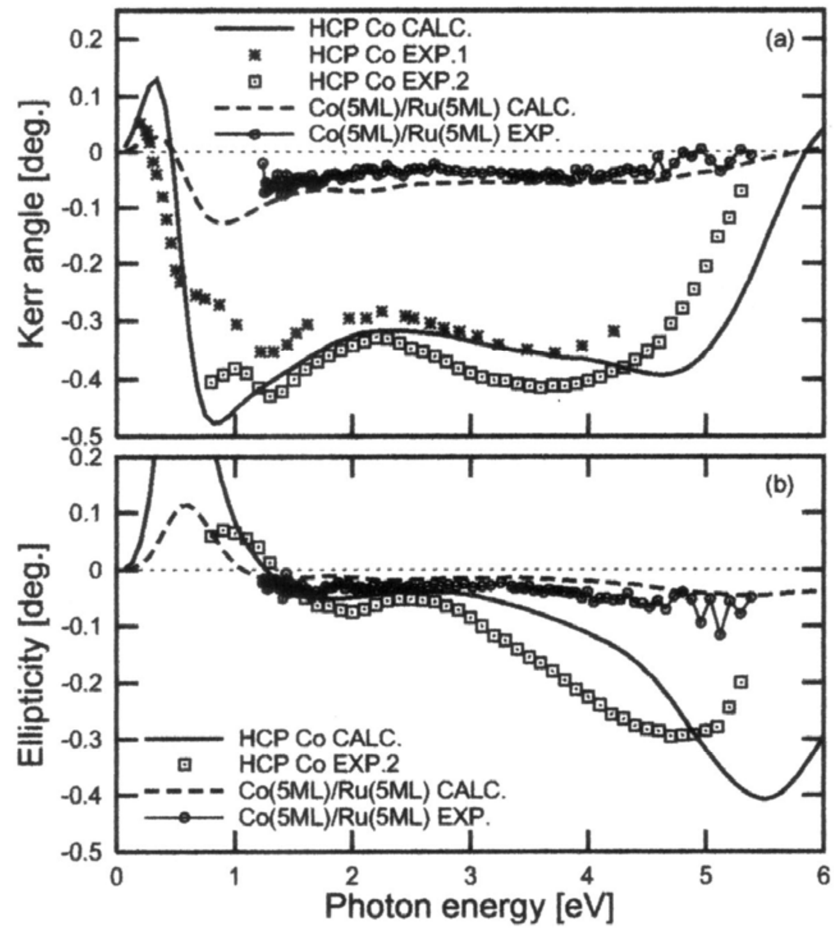

Fig. 2: The Kerr (a) and ellipticity (b) spectra of Co(5ML)/Ru(5ML) superlattice. For comparison, those of HCP Co are also shown. Experimental data of HCP Co are in Ref.[14]

NOMOKE in Co(5ML)/Ru(5ML)

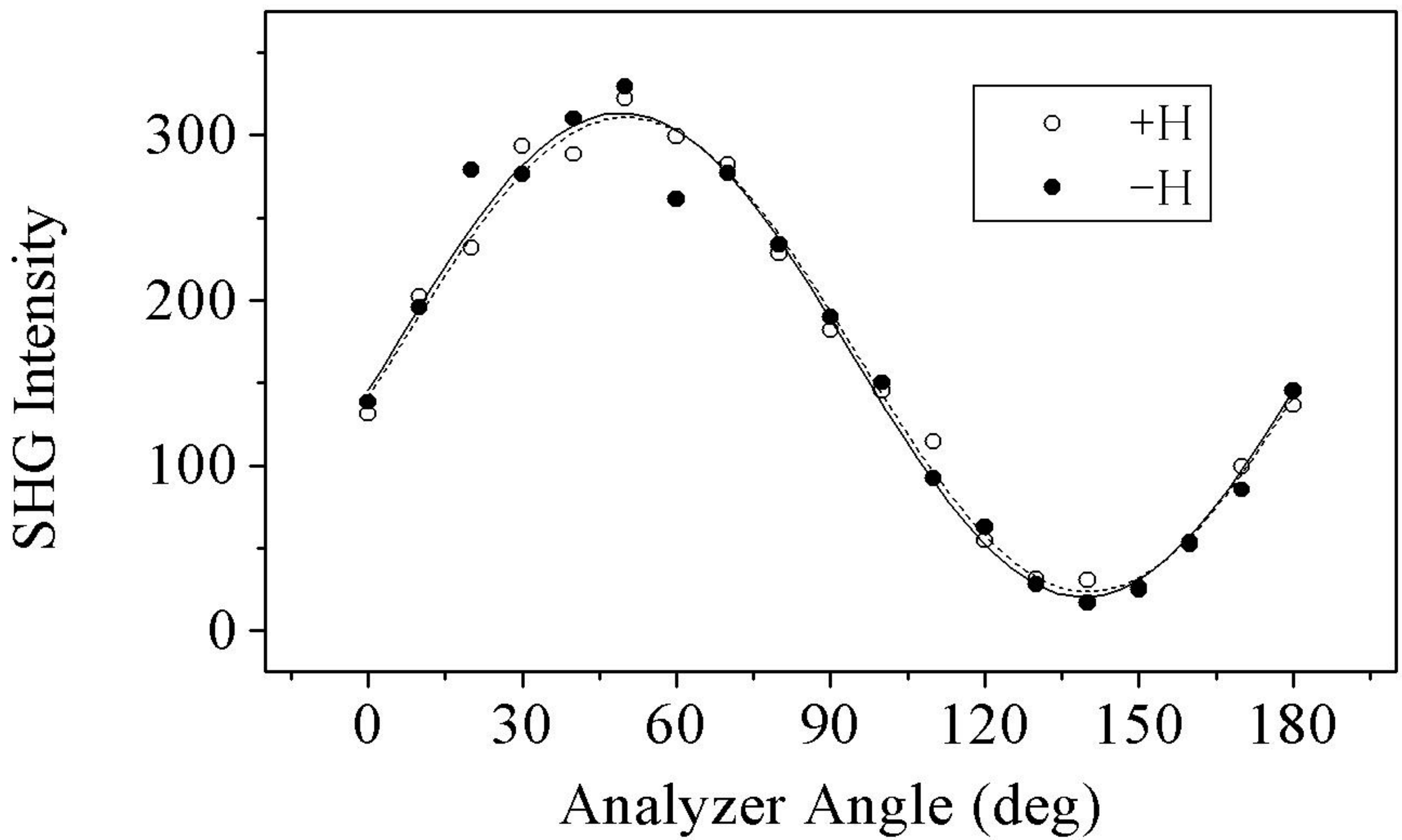

Azimuthal angle dependence of MSHG in Co(5ML)/Ru(5ML)

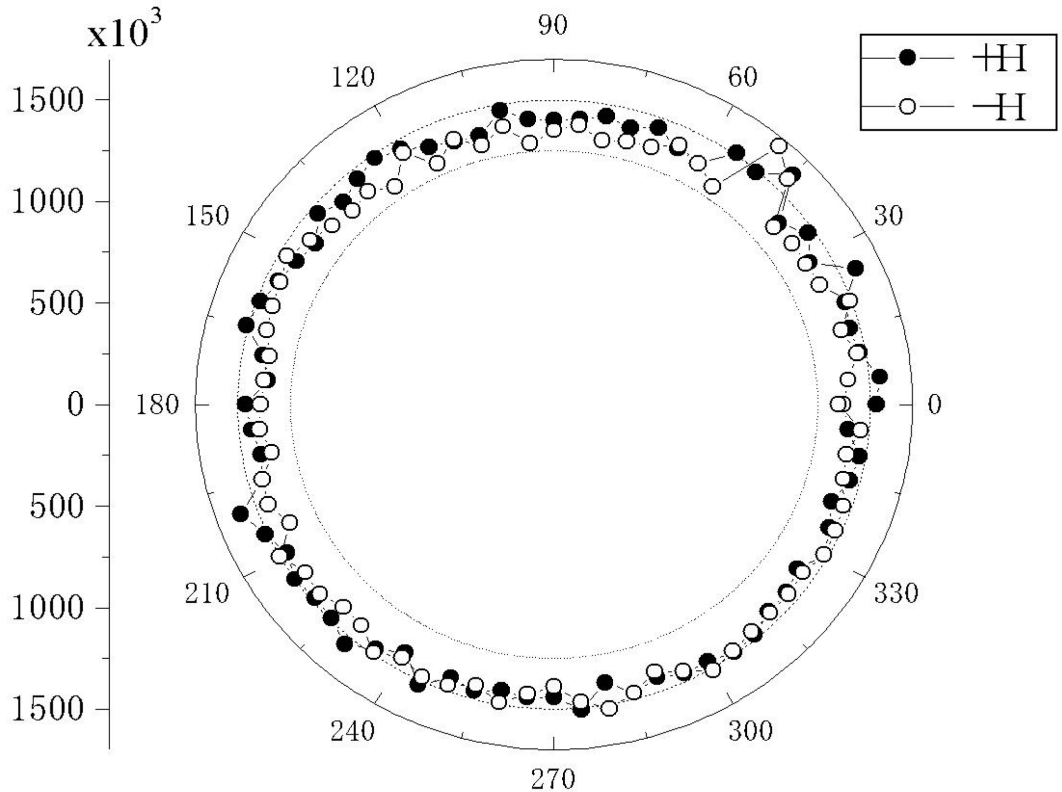

Conclusion

- Magneto-optical spectra in Fe/Cu and Fe/Au system depends strongly on the thickness of the layers in comparison with characteristic length of the material: wavelength of light, de Broglie wavelength of electrons and atomic size.

The four-fold pattern clearly reflects the symmetry of the MgO(100) substrate. This suggests that the Fe/Au superlattice is perfectly epitactic to the substrate.

- The azimuthal angle dependence was analyzed in terms of nonlinear electrical susceptibility tensor taking into account the magnetic symmetry of the superlattice.

- The azimuthal pattern was explained by symmetry analysis, taking into account the surface non-magnetic A, bulk non-magnetic B and surface magnetic C contributions.

- MSHG was shown to lead to a nonlinear Kerr rotation $\theta^{(2)}_K$ that can be orders of magnitude larger than its linear equivalent (0.2°), e.g., $\theta^{(2)}_K$ for x=1.75 was 31.1°

- We observed azimuthal angle-dependence of the nonlinear Kerr rotation for the first time.

- The azimuthal angle-dependence of the nonlinear Kerr rotation were explained using parameters determined from azimuthal patterns of MSHG response

- Modulation period dependence of parameters:
  - A (Surface nonmagnetic) is large for short period
  - B (Bulk nonmagnetic) is nearly constant
  - C (Surface magnetic) becomes larger with modulation Period.

・Magneto-optical spectra of Co/Ru superlattice are much reduced from those of Co
・This can be explained in terms of electronic hybridization of electrons between Co and Ru
・Surface magnetic effect observed by MSHG is also found to be reduced.

Linear and nonlinear magneto-optical effect offer helpful tools to investigate symmetry and electronic structure of magnetic materials

Other topics

- Near-field Magneto-optics
- XMCD

What is Near Field Optics?
近接場とは

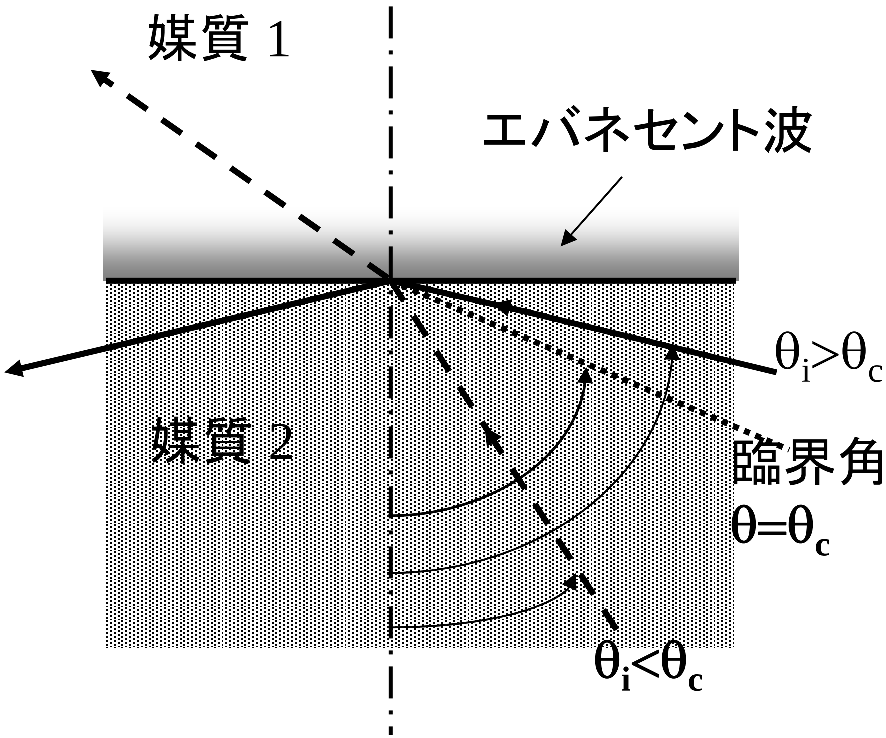

全反射とエバネセント波

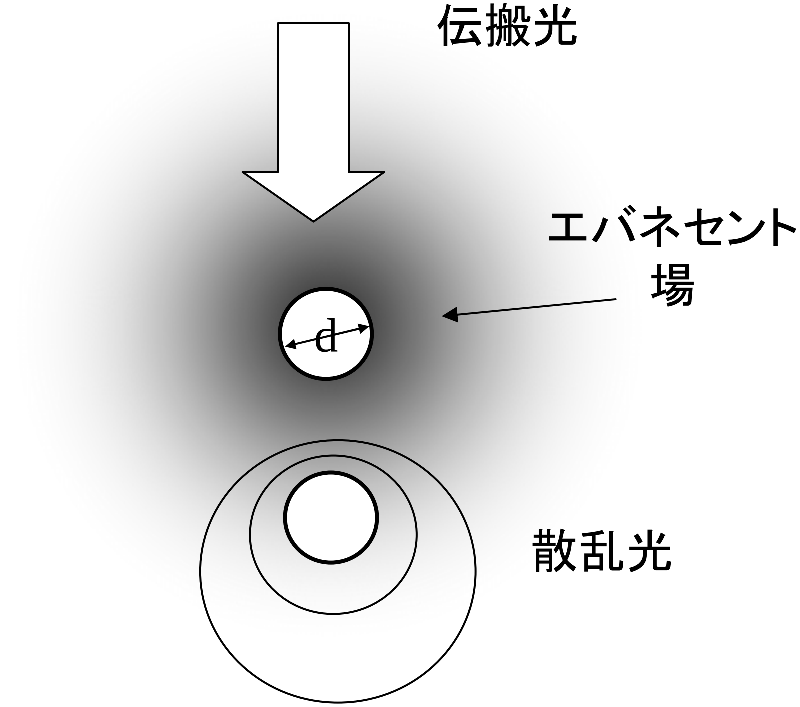

微小物体の周りのエバネセント場に置かれたもう１つの微小物体による散乱光

プローブの高さ制御

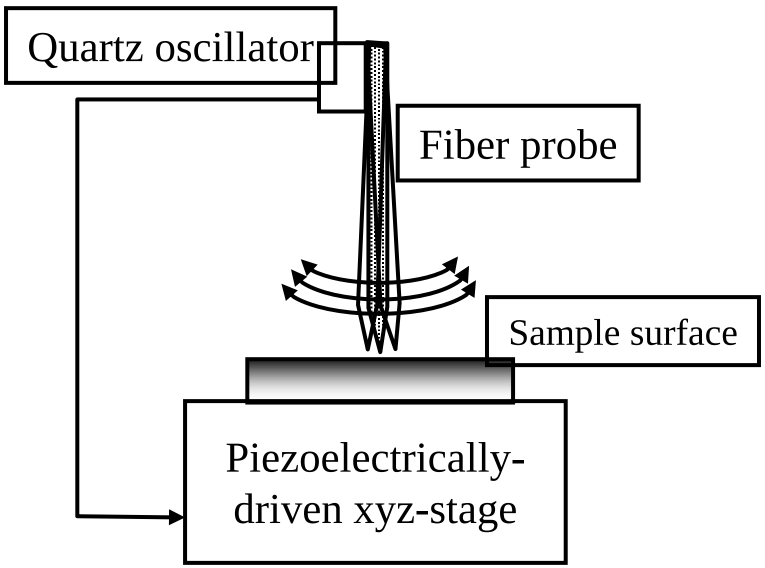
Quartz oscillator
Fiber probe
Sample surface
Piezoelectrically-driven xyz-stage

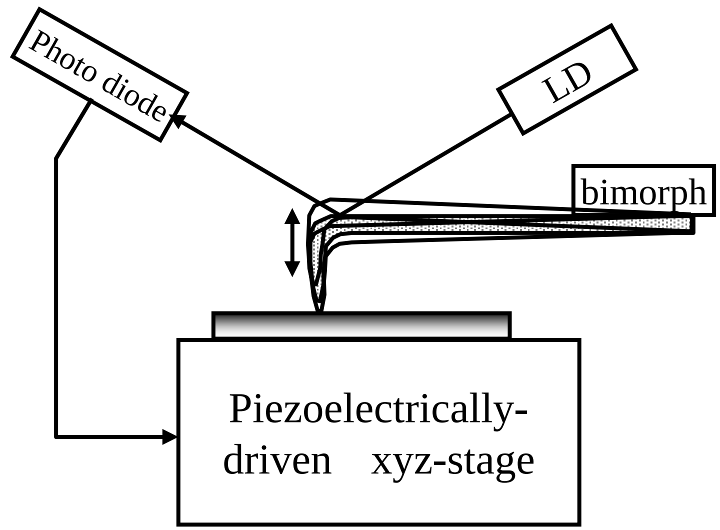
Photo diode
LD
bimorph
Piezoelectrically-driven xyz-stage

集光モード(a)と照射モード(b)

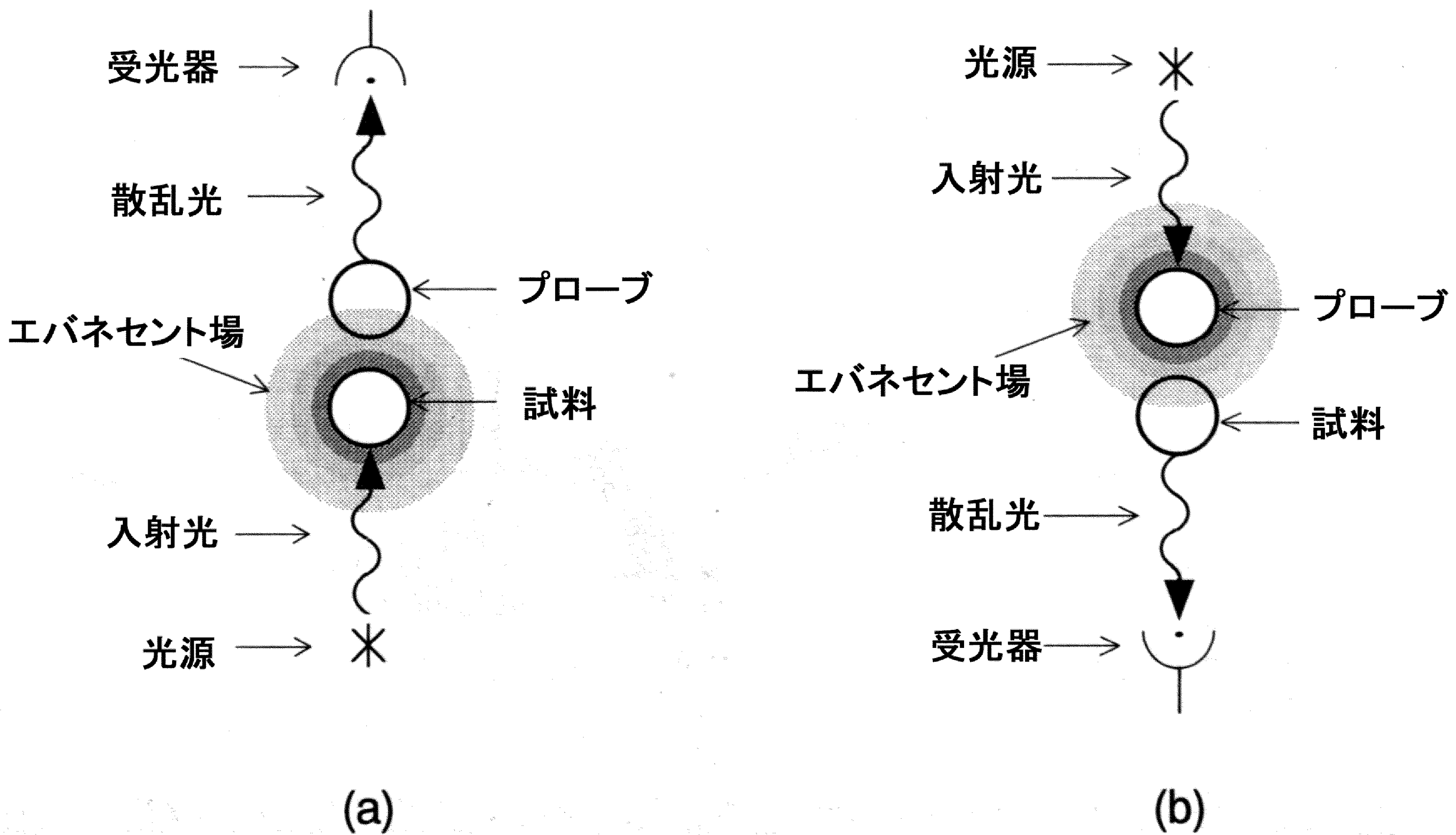

SNOMによる磁気光学測定

- 1991 Betzig : 光ファイバーをテーパー状に細めたプローブ で光磁気記録・再生に成功
- 1992 Betzig:超微細加工した金属細線リングの偏光像
- 多くの研究あるが、高解像度のMO-SNOM像は得られていない
- 偏光をファイバを通して伝えるのが困難

SNOM-AFM

- SNOM-AFMモードを利用
- はじめ：クロスニコル法→コントラスト比とれない
- 解決法：PEMによる偏光変調
- ファイバー特性の測定とよいプローブの選別
- 偏光伝達特性の補償
- 約0.1μmの解像度を達成

MO- SNOM (polarization modulation technique)

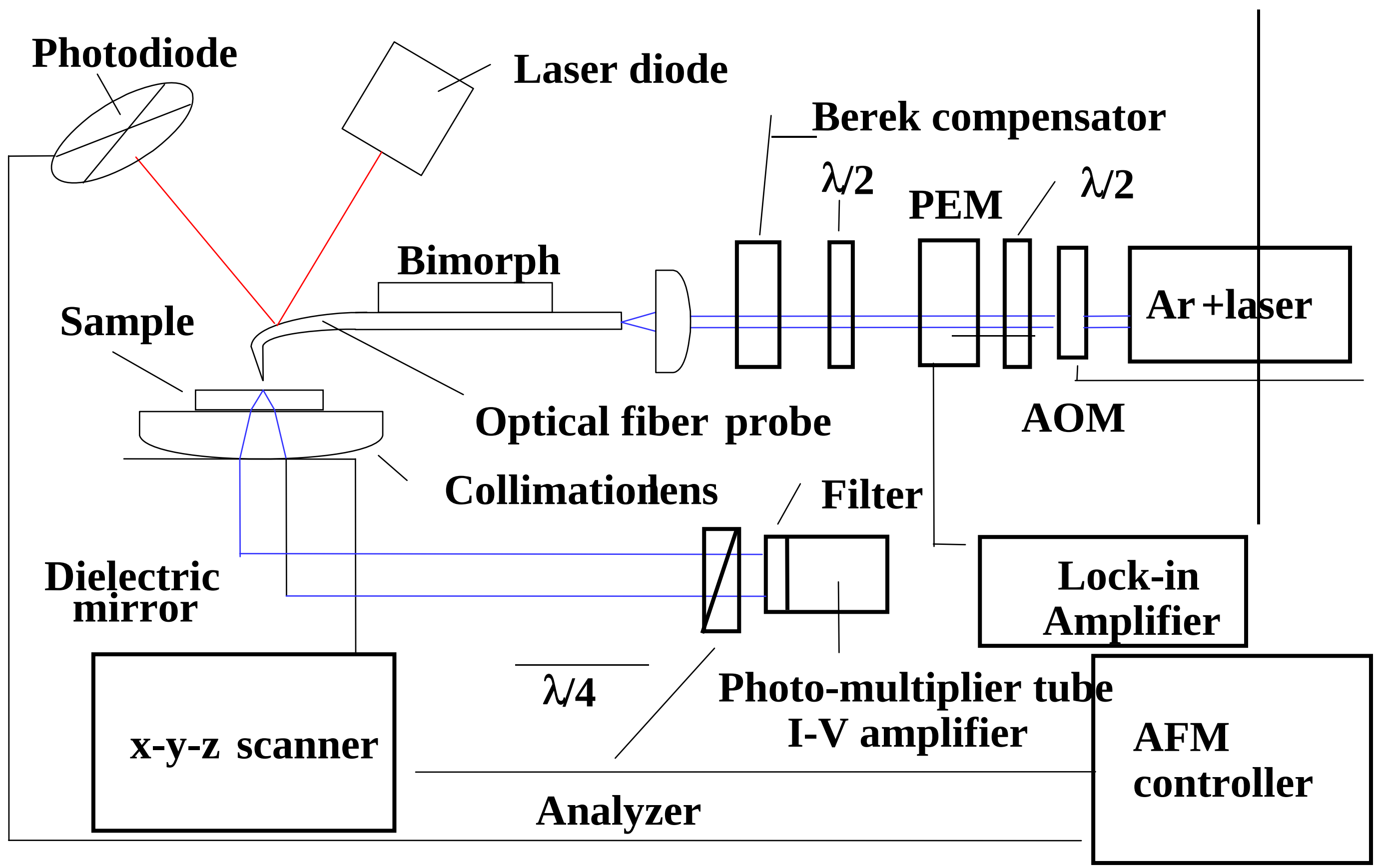

ベントファイバプローブ

Images obtained by MO-SNOM (polarization modulation technique)

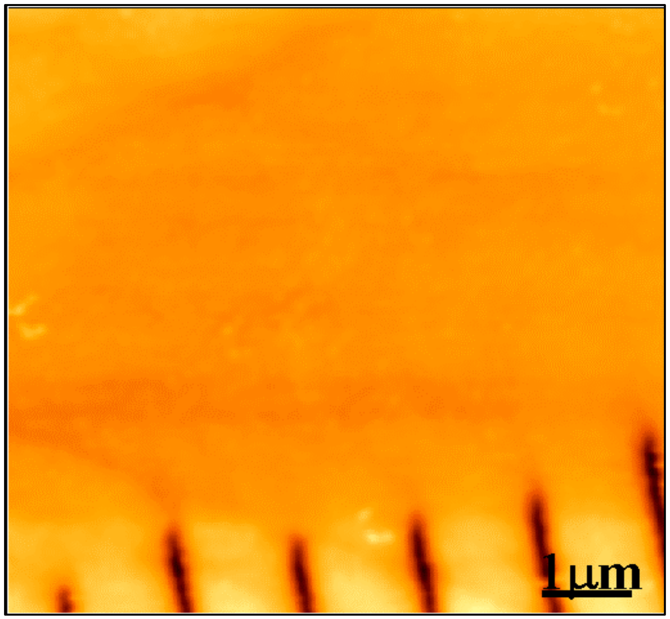

Topography

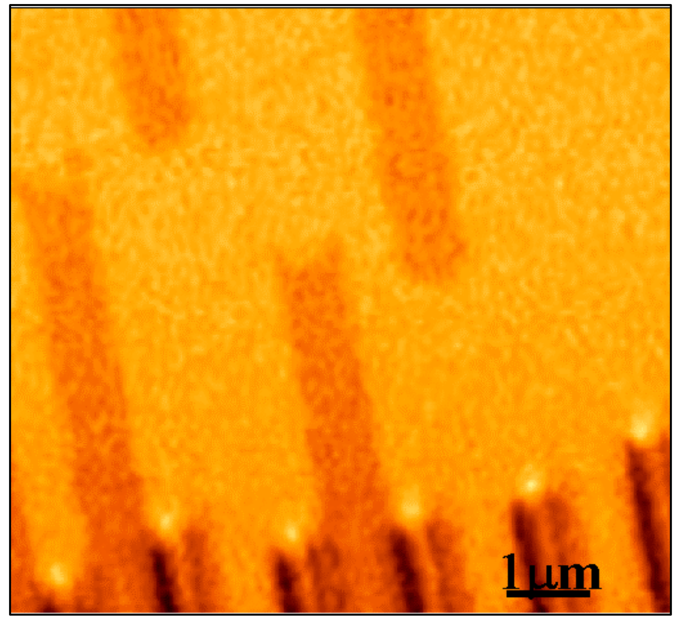

MO image

0.2μm マークのトポ像と磁気光学像

解像度の定義

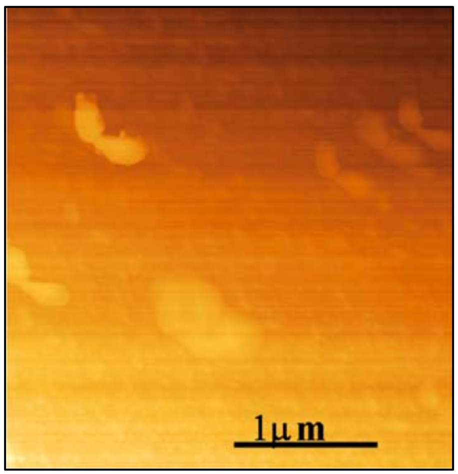

トポ像

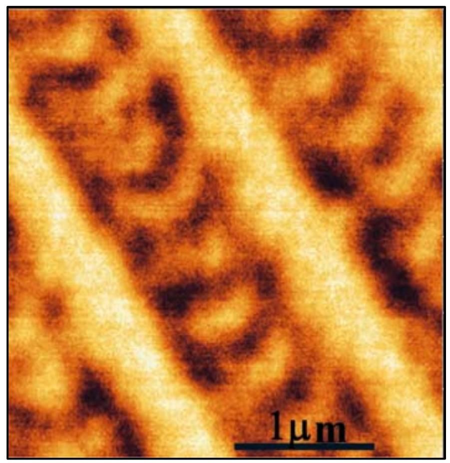

MO 像

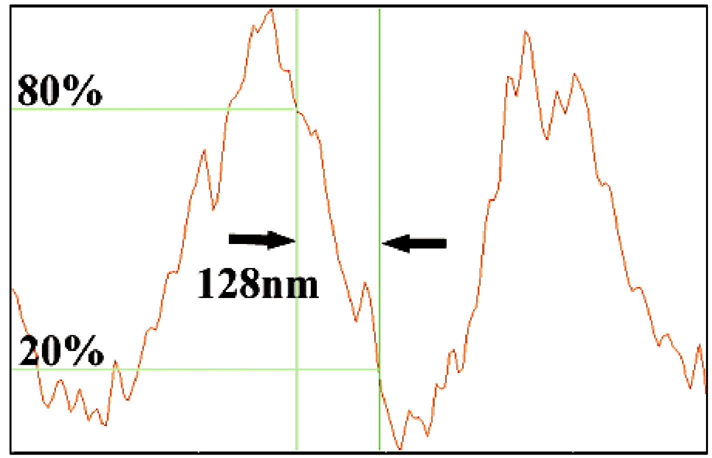

ラインプロファイル

X線磁気光学効果

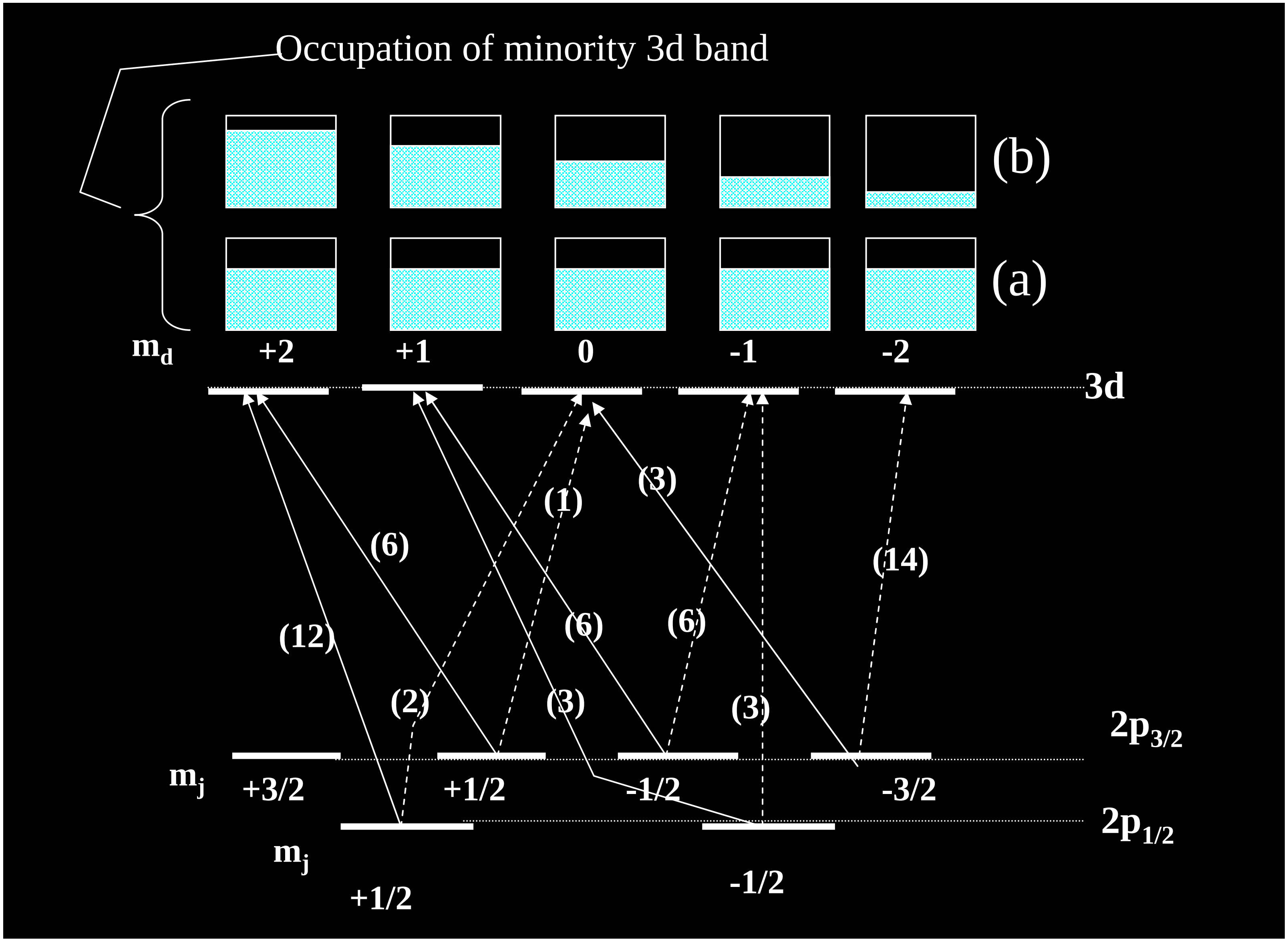
Occupation of minority 3d band
(b)
(a)
m_d
+2
+1
0
-1
-2
3d
(3)
(1)
(6)
(14)
(12)
(6)
(6)
(2)
(3)
(3)
$2p_{3/2}$
m_j
+3/2
+1/2
-1/2
-3/2
$2p_{1/2}$
m_j
+1/2
-1/2

L吸収端の磁気円二色性

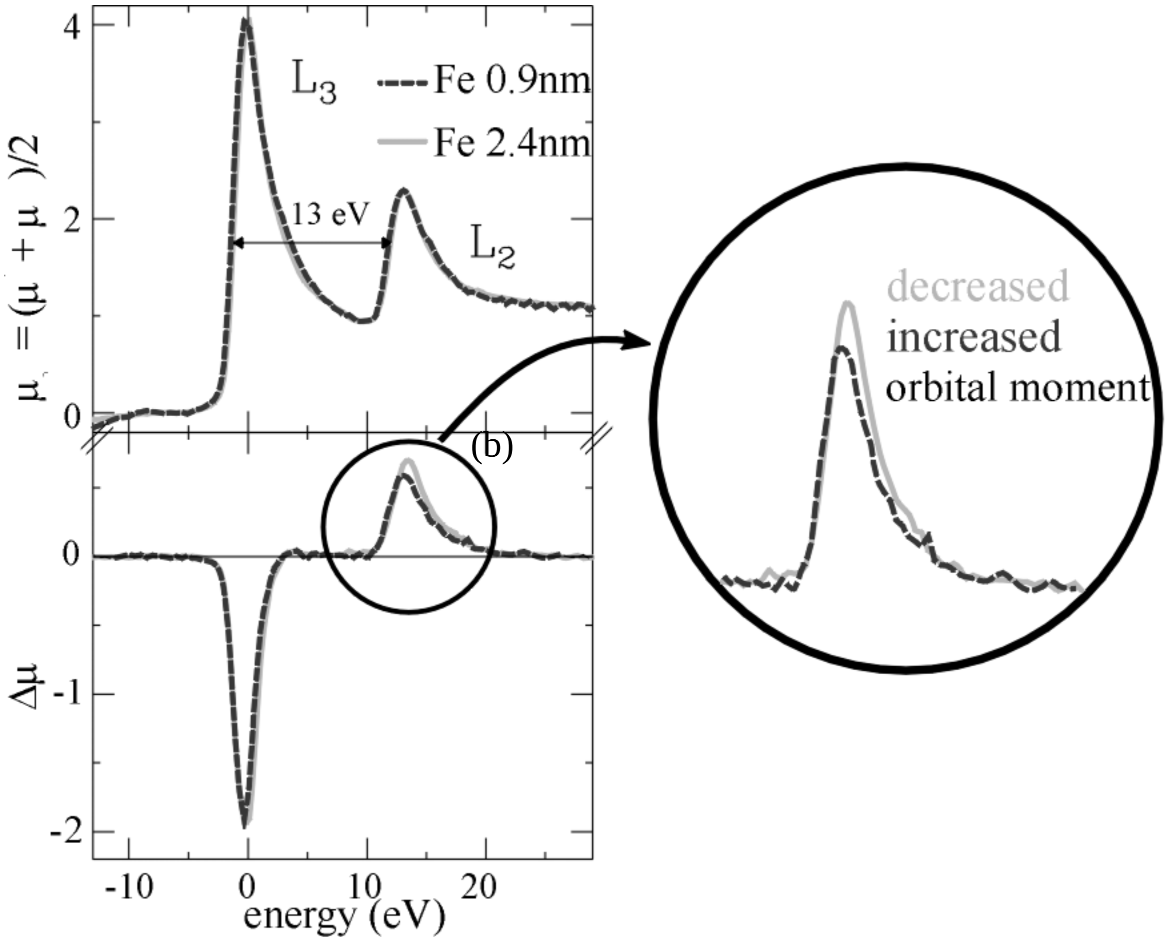

XMCD顕微鏡

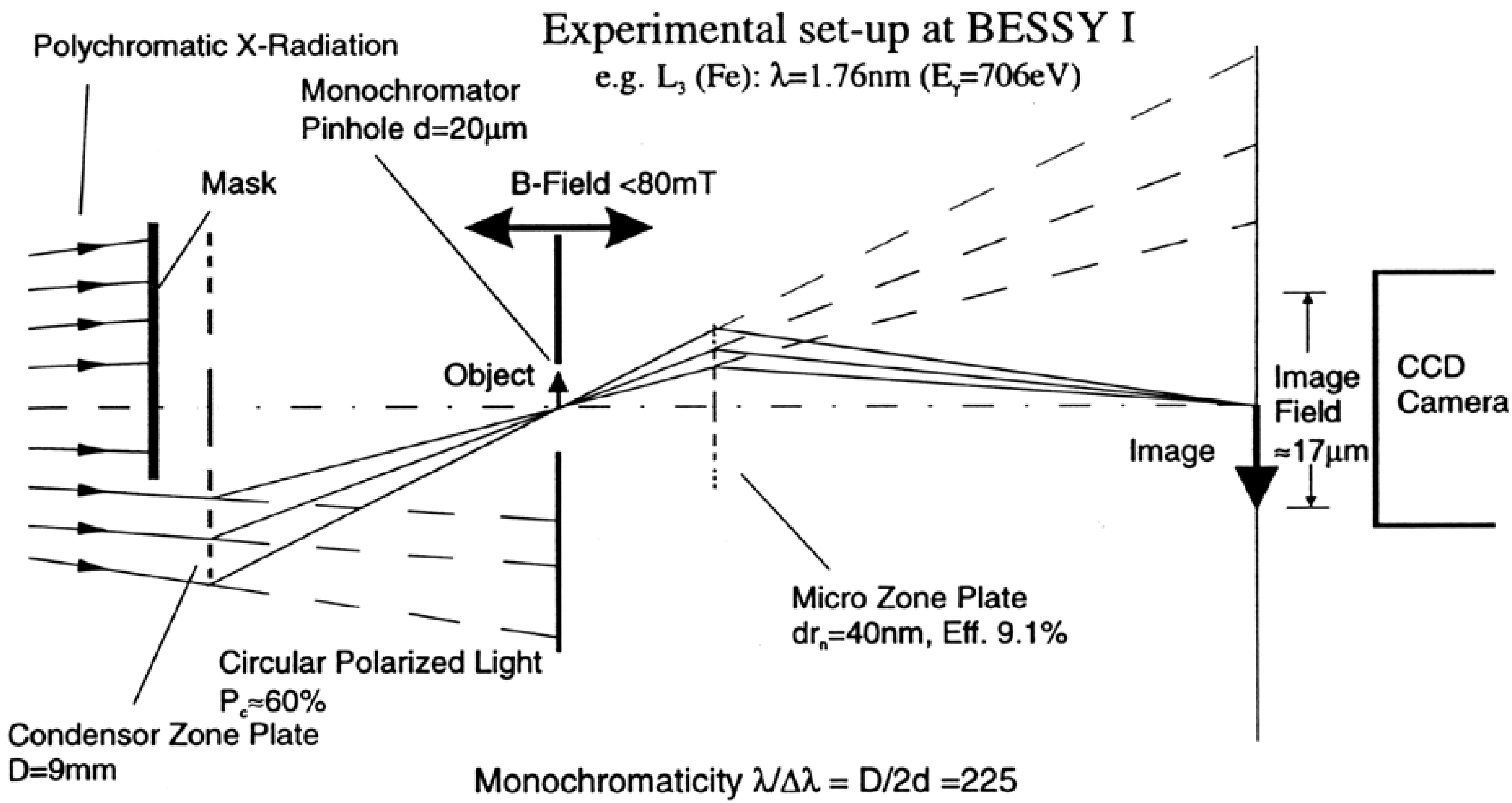
Experimental set-up at BESSY I
e.g. L3 (Fe): λ=1.76nm (Eγ=706eV)
Polychromatic X-Radiation
Monochromator
Pinhole d=20μm
Mask
B-Field <80mT
Object
Image
Field
≈17μm
CCD
Camera
Image
Micro Zone Plate
drn=40nm, Eff. 9.1%
Circular Polarized Light
Pc≈60%
Condensor Zone Plate
D=9mm
Monochromaticity λ/Δλ = D/2d =225

X線顕微鏡によるMO膜観測

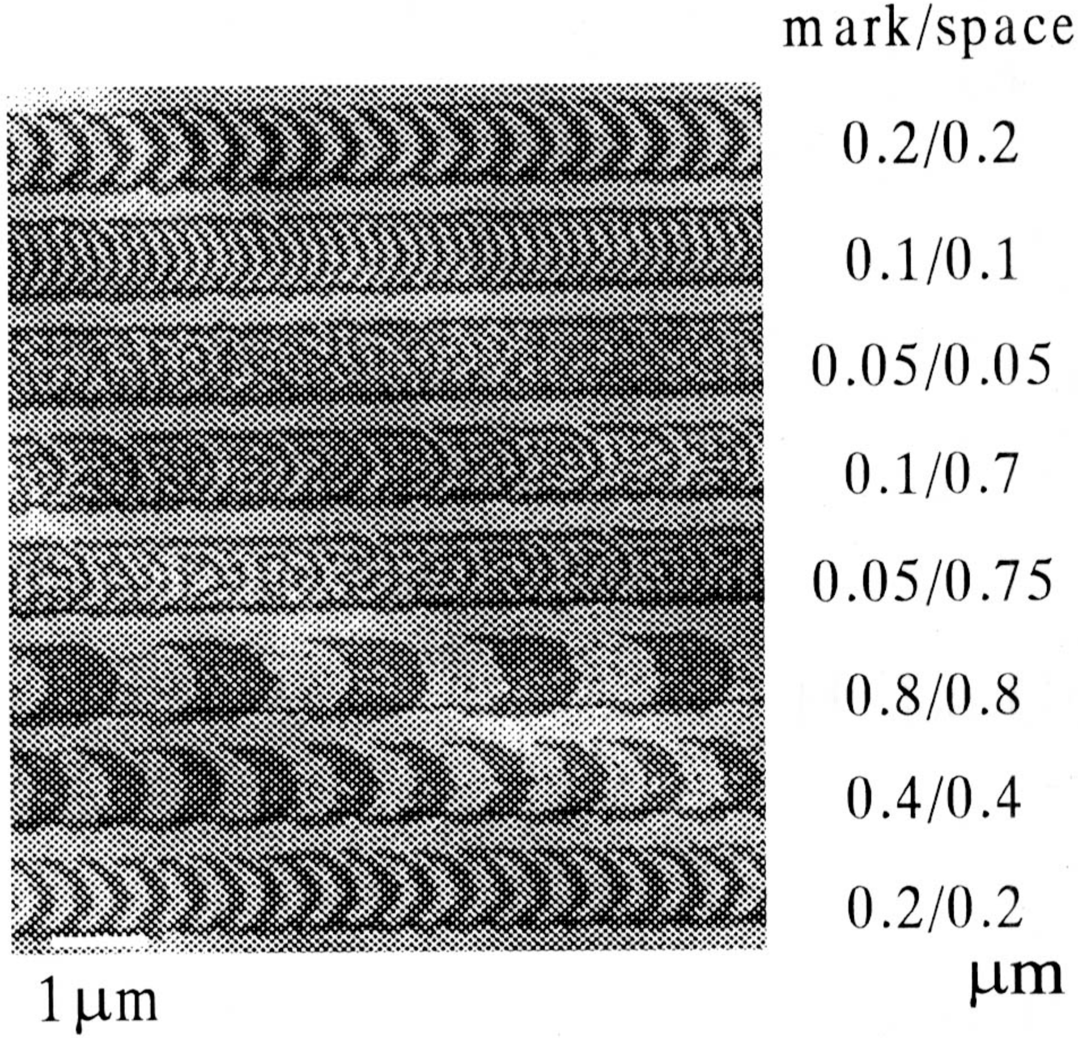

X線顕微鏡で観察したGdFeの磁区

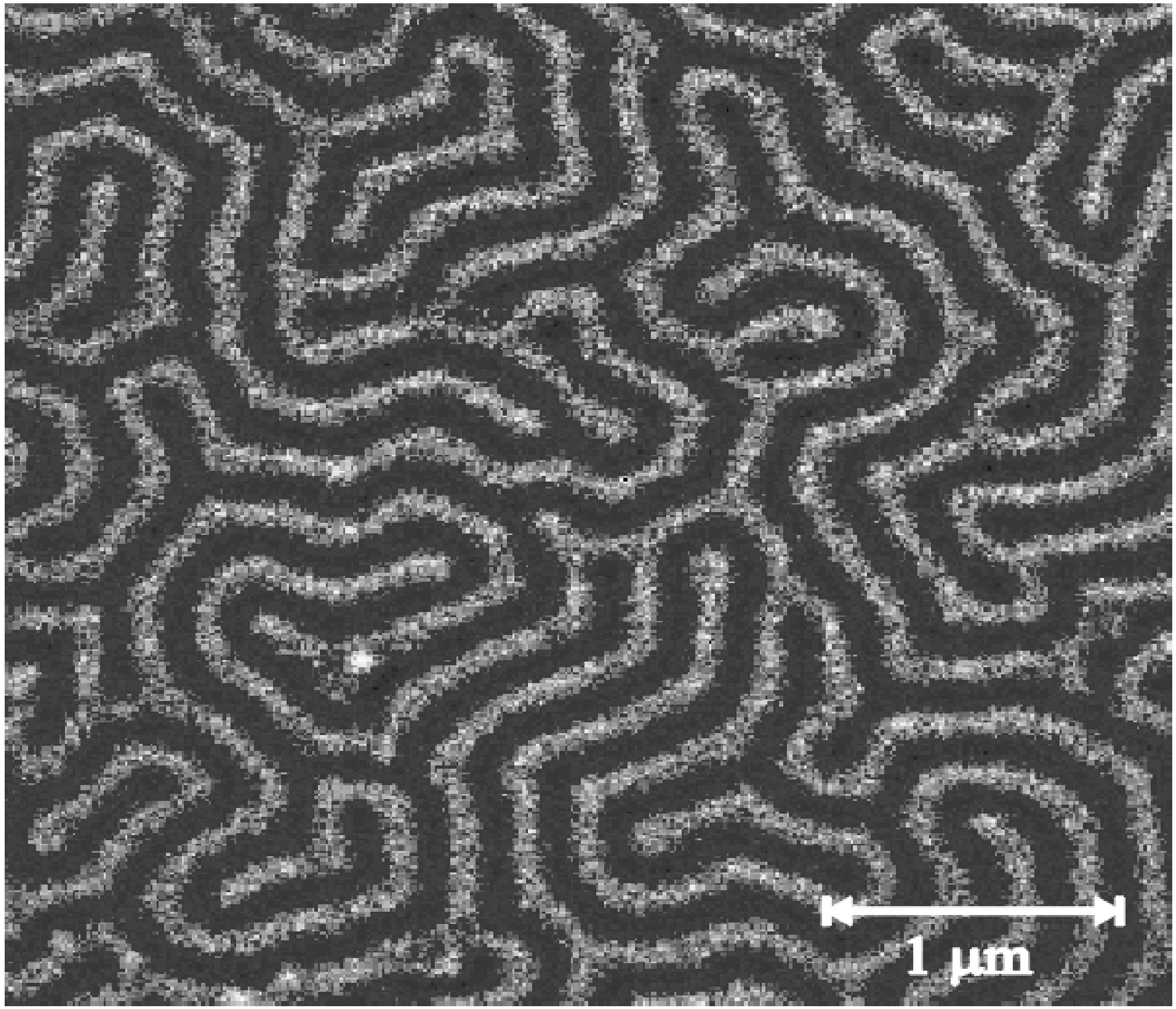

サニャック干渉計

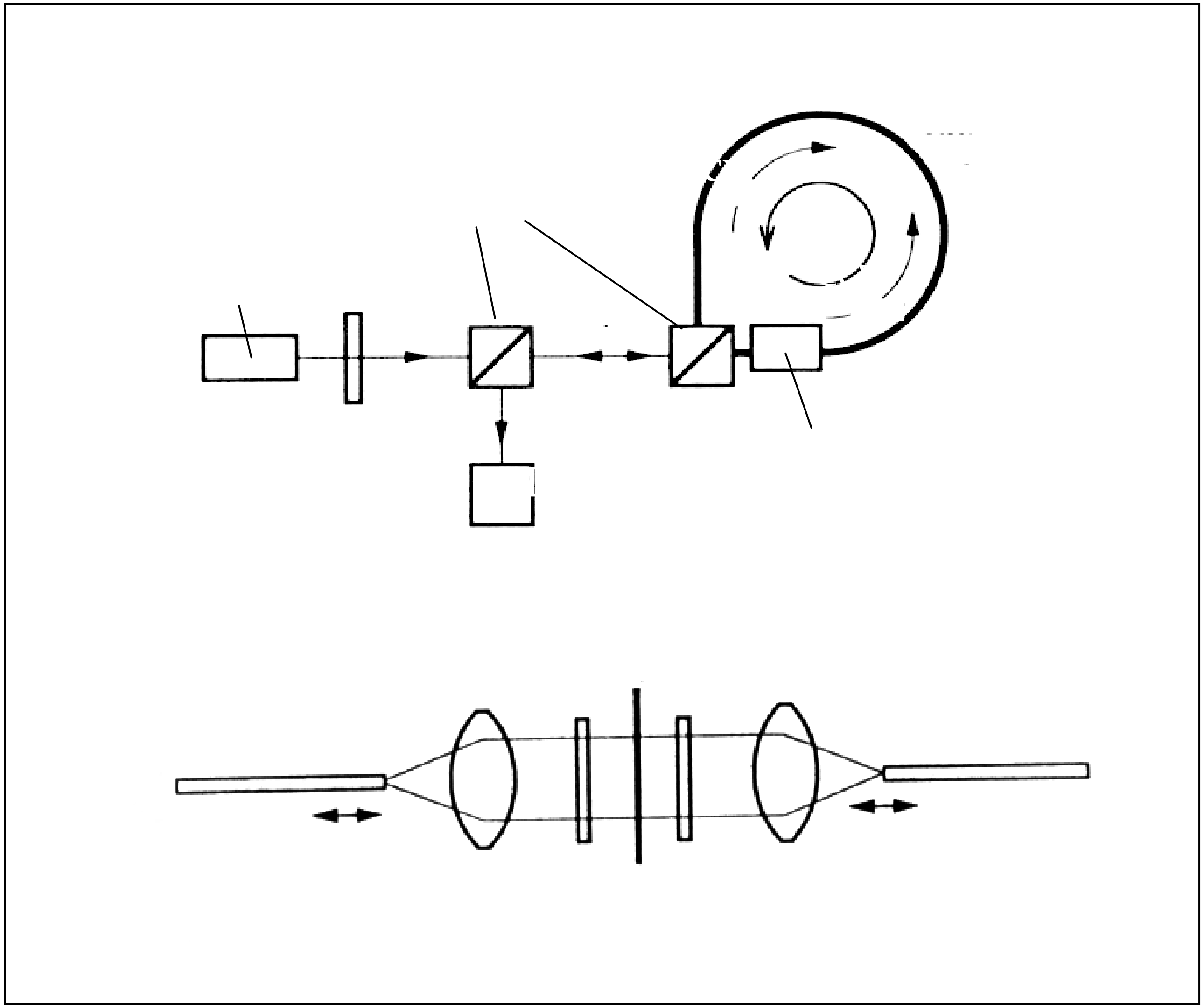

サニャックSNOM

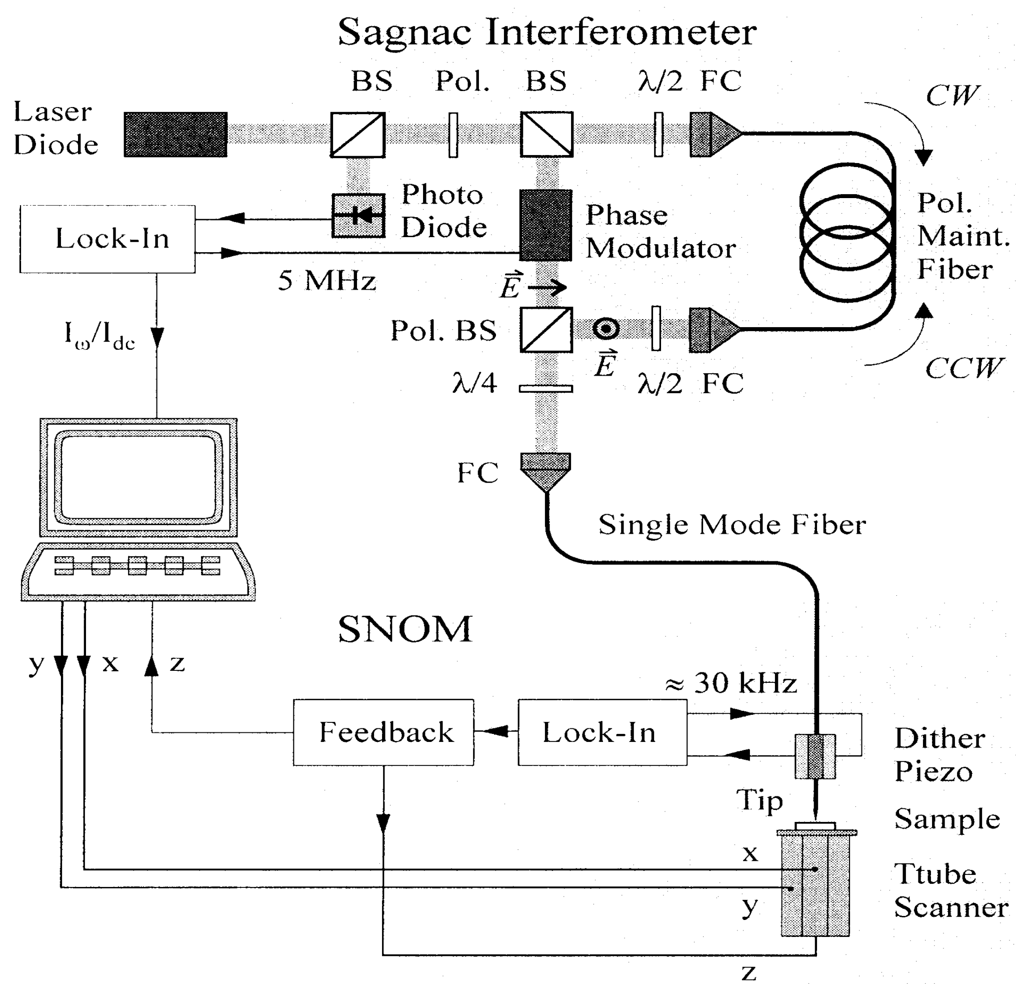
Sagnac Interferometer
BS
Pol.
BS
λ/2 FC
CW
Laser Diode
Photo Diode
Lock-In
Phase Modulator
5 MHz
Pol. Maint. Fiber
Pol. BS
λ/4
λ/2 FC
CCW
Iω/Idc
FC
Single Mode Fiber
SNOM
y
x
z
≈ 30 kHz
Feedback
Lock-In
Dither Piezo
Tip
Sample
Ttube Scanner
x
y
z

ポンププローブ磁気光学測定

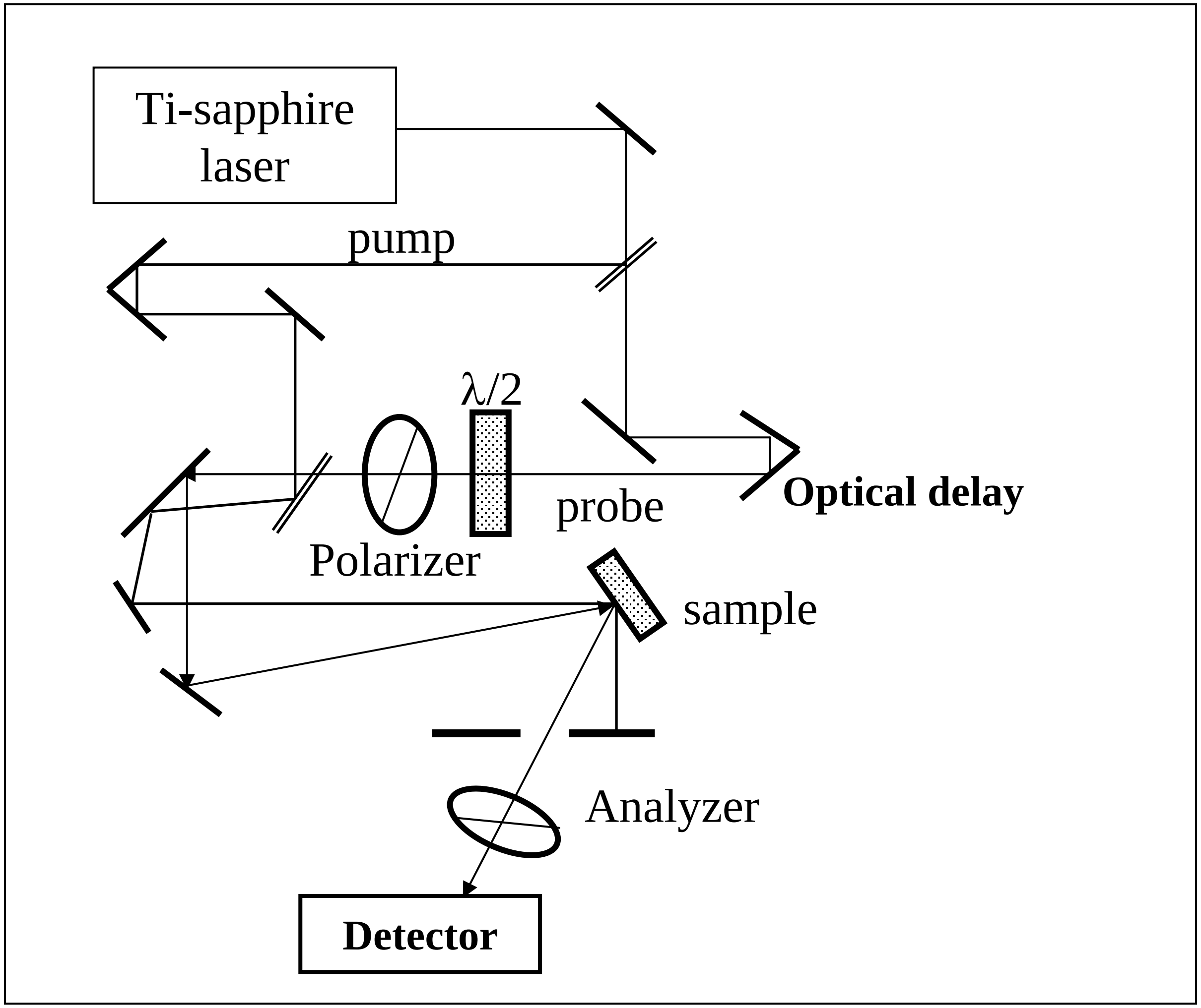

まとめ

- 磁気光学効果の基礎を、電磁気学的アプローチでのべた。この効果が誘電率テンソルの非対角成分から生じることがわかった。
- 誘電率テンソルの非対角成分は、量子論に基づいて電子エネルギー準位間の光学遷移により説明できることがわかった。
- 磁気光学スペクトルの実例を示し、それらが、電子構造から予測可能であることを示した。